

University of Alberta

Preparation of Ni/Pt Catalysts for Alkaline Alcohol Fuel Cells

by

Lise Nicole Menard



A thesis submitted to the Faculty of Graduate Studies and Research
in partial fulfillment of the requirements for the degree of

Master of Science

Department of Chemistry

Edmonton, Alberta

Fall 2008



Library and
Archives Canada

Bibliothèque et
Archives Canada

Published Heritage
Branch

Direction du
Patrimoine de l'édition

395 Wellington Street
Ottawa ON K1A 0N4
Canada

395, rue Wellington
Ottawa ON K1A 0N4
Canada

Your file *Votre référence*
ISBN: 978-0-494-47307-8
Our file *Notre référence*
ISBN: 978-0-494-47307-8

NOTICE:

The author has granted a non-exclusive license allowing Library and Archives Canada to reproduce, publish, archive, preserve, conserve, communicate to the public by telecommunication or on the Internet, loan, distribute and sell theses worldwide, for commercial or non-commercial purposes, in microform, paper, electronic and/or any other formats.

The author retains copyright ownership and moral rights in this thesis. Neither the thesis nor substantial extracts from it may be printed or otherwise reproduced without the author's permission.

AVIS:

L'auteur a accordé une licence non exclusive permettant à la Bibliothèque et Archives Canada de reproduire, publier, archiver, sauvegarder, conserver, transmettre au public par télécommunication ou par l'Internet, prêter, distribuer et vendre des thèses partout dans le monde, à des fins commerciales ou autres, sur support microforme, papier, électronique et/ou autres formats.

L'auteur conserve la propriété du droit d'auteur et des droits moraux qui protègent cette thèse. Ni la thèse ni des extraits substantiels de celle-ci ne doivent être imprimés ou autrement reproduits sans son autorisation.

In compliance with the Canadian Privacy Act some supporting forms may have been removed from this thesis.

Conformément à la loi canadienne sur la protection de la vie privée, quelques formulaires secondaires ont été enlevés de cette thèse.

While these forms may be included in the document page count, their removal does not represent any loss of content from the thesis.

Bien que ces formulaires aient inclus dans la pagination, il n'y aura aucun contenu manquant.

■+■
Canada

Abstract

A low Pt loading, Ni/Pt electrocatalyst was prepared via an evolving electrochemical co-deposition. The platinum source was the blacked platinum counter electrode. This technique produced catalysts with average platinum loadings of 1.8 at.%. The activity of the electrocatalysts towards the electrooxidation of 2-propanol in base was tested using both potentiostatic and potentiodynamic techniques. The activity of Ni/Pt towards the oxidation 2-propanol was compared to that of blacked platinum electrodes and blacked nickel electrodes under the same conditions. It was found that, at low potentials, the Ni/Pt electrocatalysts had activity similar to blacked platinum electrodes and at high potentials the Ni/Pt was more active than blacked platinum electrodes though oxidation brought on by the high potentials decreased the activity over time. Ni+Pt electrodes prepared by a conventional co-deposition technique were inactive towards the oxidation of 2-propanol.

Acknowledgements

First, I would like to thank my supervisor, Prof. Steve Bergens, for his guidance and support during my degree and for providing me with such an interesting project to pursue.

I would also like to thank the members of the Bergens Research Group, Robin Hamilton, Satoshi Takebayashi, Andrew Sullivan, Michael Hass and Dr. Corbin Ralph, for great conversations, helpful advice, and for always graciously unlocking doors for me. An especially grateful thanks is directed towards Matthew Markiewicz who spent many, many hours teaching me the fundamentals of electrochemistry, including the concept of overpotential.

Additional thanks goes out to all of my friends and relatives who have supported me with encouragement and kind listening for these past three years. Special thanks to Melanie King and Melissa King for their extraordinary friendship and to Steve Slopek, who made the decision to enter graduate school much easier.

Finally, I would like to thank my parents, Gary Menard and Diane MacDonald, and my sister Danielle Menard, whose unwavering support, love and pride have been instrumental in keeping me grounded and motivated during my toughest times.

Table of Contents

Chapter 1: Introduction	1
1.1 Introduction	1
1.1.1 What are Fuel Cells?	2
1.1.2 How Fuel Cells Work	4
1.1.3 History of Fuel Cells	6
1.2 Types of Fuel Cells	8
1.3 Direct Methanol Fuel Cells (DMFCs)	14
1.4 Direct Alcohol Alkaline Fuel Cells (DAAFCs)	17
1.5 Summary and Research Proposal	22
1.6 Conclusion	27
Chapter 2: Ni/Pt Anode Materials for the Electrooxidation of 2-Propanol in Alkaline Electrolytes	29
2.1 Electrodeposition of Anode Materials	29
2.2 Ni/Pt Anodes	34
2.3 Cyclic Voltammetry	40
2.4 CO Stripping Voltammetry	45
Chapter 3: Electrochemical Activity of Ni/Pt Electrodes Towards the Electrooxidation of 2-Propanol in Base	53
3.1 Potentiodynamic Electrooxidation of 2-Propanol	53
3.2 Potentiostatic Electrooxidation of 2-Propanol	59
3.3 Conclusion and Application to an Operational Fuel Cell	71
Chapter 4: Conventional Co-Deposition of Ni+Pt Electrodes Using Platinum Metal Salt Precursors	72
4.1 Galvanostatic Co-Deposition of Ni+Pt Electrodes	72

4.2 Voltammetry of the Co-Deposited Electrodes	79
4.3 Electrochemical Oxidation of 2-Propanol	82
4.4 Conclusion	84
Chapter 5: Future Work	86
Chapter 6: Experimental Procedures	88
Chapter 7: References	97

List of Tables

Chapter 1:

Table 1-1: Summary and comparison of the major types of fuel cells	13
--	----

List of Figures

Chapter 1:

Figure 1-1: Schematic of a hydrogen/oxygen fuel cell	4
Figure 1-2: Schematic of an alkaline fuel cell	10
Figure 1-3: Schematic of a direct methanol fuel cell	14
Figure 1-4: Schematic of a direct 2-propanol alkaline fuel cell	19

Chapter 2:

Figure 2-1: Deposition potential of the working electrode over time during blacking at -0.1 A from 0.2 M NiCl ₂ / 2.0 M NH ₄ Cl	31
Figure 2-2: Deposition potential of an electrode over time, using a graphite counter electrode, during blacking at -0.1 A from 0.2 M NiCl ₂ / 2.0 M NH ₄ Cl	32
Figure 2-3: Deposition potential of the Pt counter electrode over time during the deposition of a Ni/Pt electrode	35
Figure 2-4: Potential behavior of a Ni/Pt electrode showing the concentration of platinum in the deposition solution as a function of time	36
Figure 2-5: Average mass deposited onto Ni _{Black} electrodes and Ni/Pt electrodes	37
Figure 2-6: Average mass of Pt deposited onto Ni _{Black} electrodes and Ni/Pt electrodes	39
Figure 2-7: Decomposition of dilute H ₂ O ₂ over a Ni _{Black} electrode, a Ni/Pt electrode and a Pt _{Black} electrode	40
Figure 2-8: Cyclic voltammogram of a Pt _{Black} electrode in 0.5 M NaOH at a scan rate of 10 mV s ⁻¹	41
Figure 2-9: Cyclic voltammogram of a Ni _{Black} electrode in 0.5 M NaOH at a scan rate of 10 mV s ⁻¹	42

Figure 2-10: Cyclic voltammogram of a Ni/Pt electrode in 0.5 M NaOH at a scan rate of 10 mV s ⁻¹	44
Figure 2-11: CO stripping voltammetry on a Ni _{Black} electrode in 0.5 M NaOH sweeping at 10 mV s ⁻¹ for 2 sweeps	46
Figure 2-12: Illustration of the technique for calculating the CO stripping surface area of a Ni _{Black} electrode	48
Figure 2-13: CO stripping voltammetry on a Ni/Pt electrode in 0.5 M NaOH sweeping at 10 mV s ⁻¹ for 2 sweeps	50

Chapter 3:

Figure 3-1: Potentiodynamic electrooxidation of 1 M 2-propanol in 0.5 M NaOH at 60°C over a Pt _{Black} electrode at a scan rate of 10 mV s ⁻¹	53
Figure 3-2: Potentiodynamic electrooxidation of 1 M 2-propanol in 0.5 M NaOH at 60°C over a Ni _{Black} electrode at a scan rate of 10 mV s ⁻¹	55
Figure 3-3: Potentiodynamic electrooxidation of 1 M 2-propanol in 0.5 M NaOH at 60°C over a Ni/Pt electrode at a scan rate of 10 mV s ⁻¹	57
Figure 3-4: Potentiodynamic electrooxidation of 1 M 2-propanol in 0.5 M NaOH at 60°C over Pt _{Black} , Ni _{Black} and Ni/Pt electrodes	58
Figure 3-5: Unnormalized potentiostatic currents at 15 minutes for the electrooxidation of 1 M 2-propanol in 0.5 M NaOH at 60°C over a Pt _{Black} electrode	60
Figure 3-6: Normalized potentiostatic currents at 15 minutes for the electrooxidation of 1 M 2-propanol in 0.5 M NaOH at 60°C over a Pt _{Black} electrode	61
Figure 3-7: Unnormalized potentiostatic currents at 15 minutes for	

the electrooxidation of 1 M 2-propanol in 0.5 M NaOH at 60°C over a Ni _{Black} electrode	62
Figure 3-8: Potentiostatic electrooxidation of a Ni _{Black} electrode in 0.5 M NaOH at 60°C	63
Figure 3-9: Subtraction of the potentiostatic current obtained in the absence of 2-propanol from the potentiostatic current obtained in the presence of 2-propanol, normalized to the CO stripping surface area of the Ni _{Black} electrode	64
Figure 3-10: Unnormalized data for the potentiostatic electrooxidation of 1 M 2-propanol in 0.5 M NaOH over a Ni/Pt electrode	65
Figure 3-11: Normalized data for the potentiostatic electrooxidation of 1 M 2-propanol in 0.5 M NaOH over a Ni/Pt electrode	66
Figure 3-12: Comparison of the unnormalized potentiostatic electrooxidation currents over Pt _{Black} , Ni _{Black} and Ni/Pt electrodes	67
Figure 3-13: Comparison of the normalized potentiostatic electrooxidation currents over Pt _{Black} , Ni _{Black} and Ni/Pt electrodes	69
Chapter 4:	
Figure 4-1: Deposition potential of the electrode and the concentration of H ₂ PtCl ₆ in solution over time during galvanostatic electrodeposition at -0.1 A	74
Figure 4-2: Deposition potential of the electrode and the concentration of K[PtCl ₃ (C ₂ H ₄)]•H ₂ O in solution over time during galvanostatic electrodeposition at -0.1 A	76
Figure 4-3: Average mass deposited onto Ni _{Black} electrodes, Ni/Pt electrodes, and conventionally co-deposited Ni+Pt	

electrodes	77
Figure 4-4: Mass of Pt deposited onto the Ni/Pt electrodes (average), 133 μL of 0.01483 M H_2PtCl_6 electrode, 250 μL of 0.01483 M H_2PtCl_6 electrode, 133 μL of 0.01520 M $\text{K}[\text{PtCl}_3(\text{C}_2\text{H}_4)]\cdot\text{H}_2\text{O}$ electrode and 250 μL of 0.01520 M $\text{K}[\text{PtCl}_3(\text{C}_2\text{H}_4)]\cdot\text{H}_2\text{O}$ electrode	79
Figure 4-5: Cyclic Voltammograms of the four conventionally co-deposited electrodes	81
Figure 4-6: Potentiodynamic electrooxidation of 1 M 2-propanol in 0.5 M NaOH over a co-deposited Ni+Pt electrode	83
Figure 4-7: Potentiostatic electrooxidation of 1 M 2-propanol over a co-deposited electrode	84

List of Symbols and Abbreviations

at. %	atomic percentage	
cc	cubic centimeter	cm ³ , ml
ΔG	Gibbs free energy change	kJ/mol
ΔH	enthalpy change	kJ/mol
ΔS	entropy change	kJmol K
η	efficiency	
E°	standard potential	mV, V
E°_a	standard anode potential	mV, V
E°_c	standard cathode potential	mV, V
F	Faraday constant	96485 C/ mol e ⁻
M	molarity	mol L ⁻¹
T	temperature	°C, °K
AFC	Alkaline Fuel Cell	
DAAFC	Direct Alcohol Alkaline Fuel Cell	
DMFC	Direct Methanol Fuel Cell	
EDX	Energy Dispersive X-Ray Analysis	
ICE	Internal Combustion Engine	
ICP	Inductively Coupled Plasma	
LEISS	Low Energy Ion Scattering Spectroscopy	
MCFC	Molten Carbonate Fuel Cell	

MOR	Methanol Oxidation Reaction
NHE	Normal Hydrogen Electrode
ORR	Oxygen Reduction Reaction
PAFC	Phosphoric Acid Fuel Cell
PEM	Polymer Electrolyte Membrane
PEMFC	Polymer Electrolyte Membrane Fuel Cell
SCE	Saturated Calomel Electrode
SEM	Scanning Electron Microscopy
SHE	Standard Hydrogen Electrode
SOFC	Solid Oxide Fuel Cell
UV	Ultra Violet
XPS	X-Ray Photoelectron Spectroscopy
XRF-EDX	X-Ray Fluorescence – Energy Dispersive X-Ray Analysis

Chapter 1: Introduction

1.1 Introduction: Global warming is a major international concern because of current, rather alarming, warming trends. Initiated by the industrialization of current first world nations, these warming trends will only amplify with increased industrialization in the third world and because of the projected dramatic increase in automobile use in developing, large economies such as in China and India. For example, the recently released Tata Nano,¹ a small, \$2500, 4-passenger vehicle from India, threatens to dramatically increase car ownership at significant cost to the environment. Similarly, China's hunger for economic growth has created a reliance on coal burning plants for energy generation. These plants operate on dirty coal that contains many toxic impurities such as sulfur and that releases incredible volumes of harmful emissions.² The 2007 Nobel Peace Prize was awarded to the Intergovernmental Panel on Climate Change and Albert Gore Jr. for "their efforts to build up and disseminate greater knowledge about man-made climate change, and to lay the foundations for the measures that are needed to counteract such change".³ Toxic emissions of gases such as CH₄, NO_x, SO_x, CO₂, and carbon particulates into the atmosphere are strongly believed to contribute to the increase in global temperature.⁴ Many of these toxic emissions are produced via the combustion of fossil fuels in traditional internal combustion engines (ICEs) used for transportation, heat and energy

generation.⁴ As a result, a good deal of current research is directed towards reducing greenhouse gas emissions and smog through the discovery and development of efficient processes for energy production that provide high power densities with minimal harmful effects on the environment. Fuel cells are, in principle, capable of providing such a solution.

1.1.1 What are Fuel Cells?: Fuel cells are electrochemical devices that convert the free energy of a chemical reaction directly into electrical energy.⁵ Fuel cells are a leading alternative for energy storage and production in portable electronics and transportation. Fuel cells produce no toxic emissions, run quietly, and do not contain large numbers of moving parts.⁶ Their modular design allows them to be stacked in series to meet a variety of energy requirements, and they require relatively little maintenance.⁶

The Carnot Cycle governs the maximum theoretical operating efficiency of traditional ICEs. The Carnot Efficiency equation states that the efficiency by which heat is converted into mechanical energy is directly limited by temperature.⁵ This efficiency, η , obtained by the Carnot equation is idealized, and T_1 and T_2 are the input and output temperatures, in degrees Kelvin, respectively.

$$\eta = \frac{T_1 - T_2}{T_1} \qquad \text{Eq. 1-1}$$

In practice, real efficiencies of operating ICEs are lower than ideal Carnot efficiencies due losses to friction, etc., during the energy conversion processes. As a result, typical ICEs have low efficiencies.

Unlike heat engines, the efficiency of fuel cells is not limited by the Carnot Cycle. Fuel cells convert the free energy of the chemical reaction, ΔG , directly into electrical energy at a constant temperature. The efficiency of a fuel cell is a measure of the energy produced in relation to the enthalpy change, ΔH , of the reaction. The related equations are shown below where η is the efficiency, n is the number of moles of electrons involved in the reaction, F is the Faraday constant (96487 C mol^{-1}), ΔG is the Gibbs free energy of the system, and E° is the standard cell potential.

$$\eta = \frac{\Delta G}{\Delta H} \quad \text{Eq. 1-2}$$

$$\Delta G = -nFE^\circ \quad \text{Eq. 1-3}$$

$$\eta = -\frac{nFE^\circ}{\Delta H} \quad \text{Eq. 1-4}$$

Since the free energy and enthalpy of fuel cell reactions are often close in magnitude, fuel cells have ideal efficiencies near 100%. In some cases the ideal efficiency of a fuel cell can surpass 100%. This occurs when ΔG of the reaction is greater than the ΔH of the reaction. Efficiencies greater than 100% are possible because the fuel cell absorbs heat energy from the surroundings and incorporates it into the overall energy output. The Gibbs free energy is related to the entropy, ΔS , of the system according to the equation:

$$\Delta G = \Delta H - T\Delta S$$

Eq. 1-5

Chemical reactions that have negative values for ΔS will lead to ΔG values more positive than ΔH . Such is the case for the reaction of carbon and oxygen to form CO, and the theoretical efficiency for this reaction is 124% at standard temperatures and pressures (0°C and 1 atm).⁷

1.1.2 How Fuel Cells Work: All fuel cells consist of four main components: the anode (negative electrode), the cathode (positive electrode), an electrolyte layer located between them that allows for ion migration, and an external circuit. The principles of fuel cell operation can be demonstrated using a hydrogen/oxygen fuel cell as an example. Figure 1-1 is a simplified schematic of the processes occurring in a fuel cell operating on hydrogen and oxygen.

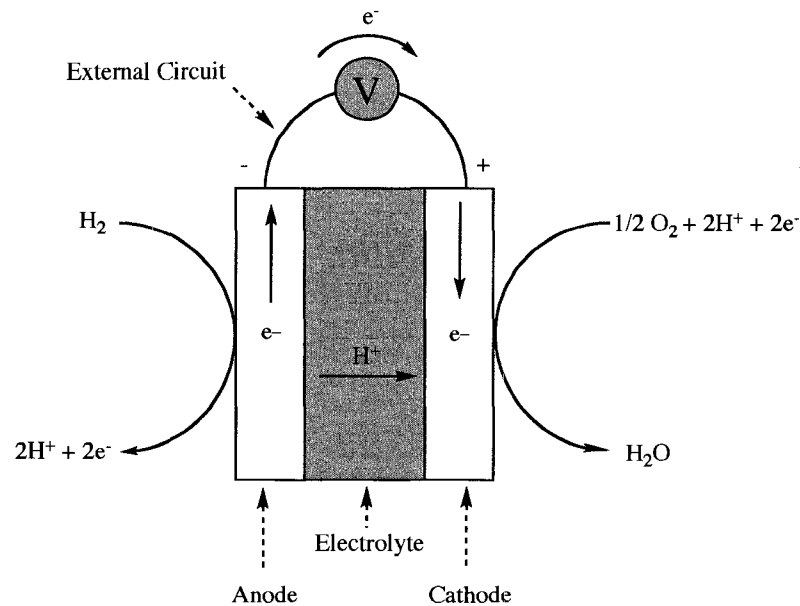


Figure 1-1: Schematic of a hydrogen/oxygen fuel cell.

Hydrogen (fuel) is oxidized at the anode to form protons and electrons. The protons migrate through the electrolyte towards the cathode (ionic conduction), while the electrons travel in the same direction through an external circuit. At the cathode, oxygen (from air) is reduced by the electrons and reacts concomitantly with the protons to form water. Water is removed from the fuel cell at the cathode exhaust. Precious metal electro-catalysts are required at both the anode and cathode. Without precious metal electro-catalysts at the electrode interfaces, the kinetics of the reactions proceed too slowly. The half-reactions and overall cell reactions are shown below:



The ΔG of reaction is the driving force for the electrons to travel through the external circuit and thereby allows fuel cells to provide power.

Prototype hydrogen fuel cells have been operated at 80% efficiency,⁸ so in principle, such cells would be an integral component of a hydrogen economy. They produce electrical energy in high efficiency with only water and some heat as byproducts. Fuel cells do not produce toxic emissions such as SO_x , NO_x , CO_2 or carbon particulates. There are, unfortunately, several formidable challenges that currently prevent the adoption of hydrogen fuel

cells for mainstream use. One challenge is the complex issue of hydrogen storage and transportation.⁹ Hydrogen gas has a lower energy density than liquid fuels at standard operating temperatures, and so must be stored under high pressures. Compressing hydrogen to high pressures requires substantial energy that must be subtracted from the energy stored in the hydrogen. Pressurized cylinders possess an inherent safety risk, and they present a physical barrier because of their large size and weight.⁹ Additionally, the need for high-pressure hydrogen tank refill stations, and components such as gas regulators to handle high-pressure hydrogen, pose serious safety concerns. Further, significant political and economic barriers exist to the development of a hydrogen infrastructure.⁹ In addition, hydrogen is not readily available; currently it can only practically be produced on large scales by reforming carbon based fuels.¹⁰ A third limitation is the high cost of the electro-catalysts currently required for efficient operation.

1.1.3 History of Fuel Cells:^{5,11,12} Sir William Grove created the first fuel cell in 1839. Using platinum electrodes, hydrogen and oxygen gas, and a sulfuric acid electrolyte, Grove successfully ran the reaction of hydrogen and oxygen to produce water and electricity.¹³ At this time, fuel cells were considered more of a curiosity than a practical energy source. Immediate subsequent work focused on improving the efficiency of the platinum electro-catalysts.¹¹ In 1894 Ostwald proposed that extracting energy from coal electrochemically rather

than via combustion would allow the use of a greater percentage of the energy in the coal.¹⁴ This set in motion work on direct coal fuel cells. Preliminary work on solid oxide and molten carbonate fuel cells began in the 1930's and, in 1939, Francis Bacon developed an alkaline fuel cell using nickel electrodes and a potassium hydroxide electrolyte.¹⁵ The design was improved in 1954 when pores were introduced into the electrode materials to help control pressure and a corrosion resistant cathode was prepared from lithium doped nickel oxide.¹¹ NASA's Apollo space missions in the 1960's were powered by alkaline fuel cells based largely on Bacon's design. The energy produced provided electricity for the guidance, communication and life support systems while providing drinking water for the flight crew.¹⁶ At the same time, Shell® and Esso® were developing direct methanol fuel cells using aqueous acidic electrolytes,¹¹ which paved the way for polymer electrolyte membrane fuel cells (PEMFCs).

Fuel cells were first used to power vehicles in the 1950s; the following are select highlights from the history of fuel cells used for transportation. The first fuel cell powered vehicle was the Allis-Chalmers Manufacturing Company's alkaline fuel cell (AFC) powered tractor in 1959.¹⁷ This was followed in 1967 by the General Motors Electrovan, which employed an AFC system where the H₂ and O₂ fuels were stored onboard in cryogenic tanks.¹⁸ In the 1990s, both Ballard Power Systems and Daimler-Benz introduced a multitude of vehicles operating on solid polymer fuel cell systems.¹⁶ Today,

solid polymer (PEM) fuel cells are considered the most appropriate cell type for use in transportation applications because of their low operating temperatures, durability, and lightweight cell designs.¹⁹

1.2 Types of Fuel Cells:^{20,21,22}

Fuel cells are usually classified by the type of electrolyte they employ. Below, the most common types of fuel cells are discussed.

Polymer Electrolyte Membrane Fuel Cells (PEMFCs):^{19,23,24} These cells are also called Proton Exchange Membrane Fuel Cells. They operate using a thin, solid, ion-exchange membrane between the electrodes. Hydrogen gas is supplied to the anode where it is oxidized into protons and electrons. The protons travel from the anode to the cathode through the electrolyte membrane while the electrons travel through an external circuit. Oxygen is reduced at the cathode to form water. Compared to other types of fuel cells, PEMFCs operate at lower temperatures, around 80°C, they have typical efficiencies between 40-60%, have rapid start-up, they are lighter, more portable, and they are more compact.¹⁹ Additionally, the solid electrolyte (as opposed to liquid) allows for better sealing, and for less cell corrosion, thus increasing the cell's longevity.²³ The major drawback with these systems, however, is that PEMFCs only work well at low temperatures using hydrogen

as fuel.²⁰ When operating on hydrogen, the major factor that decreases the performance of acidic PEMFCs is the slow kinetics of oxygen reduction at the cathode.¹⁹ The most applicable method to overcome this limitation is to use high loadings of expensive, precious metal electro-catalysts, though new deposition techniques have, to an extent, helped in reducing the required loads.²⁴ Furthermore, water transport through the electrolyte must be carefully monitored and controlled. To ensure proper hydration and proton mobility, the fuel must be humidified and the electrolyte must not be allowed to dry out. An excess of water at the cathode, however, will flood the electrolyte-electrode interface, blocking the cathode catalyst, and decreasing the cell's performance. Poisoning of the electrode by CO is another disadvantage of PEMFC design.²⁰ Current and foreseeable large-scale sources of hydrogen are produced through natural gas or CH₄ reforming.^{25,26} The reforming process creates trace CO that must be carefully removed from the fuel because CO poisons the platinum metal at the anode. A great deal of effort has been invested in the development of CO resistant anode materials.²⁷ Direct Methanol Fuel Cells (DMFCs), a type of PEMFC, will be discussed in a further section.

Alkaline Fuel Cells (AFCs):^{17,28} These low temperature fuel cells operate between 60°C and 90°C and use aqueous potassium hydroxide as the electrolyte. A major advantage of AFCs is that the kinetics of oxygen reduction

at the cathode are faster than acidic systems.²¹ Further, non-precious metals (often nickel) can be used as electro-catalysts.¹⁷ Hydrogen gas and oxygen gas are supplied to the anode and cathode respectively. Alkaline fuel cells are used in space shuttles because they are lighter and less corrosive than their acidic counterparts. Figure 1-2 shows the simplified schematic of an AFC operating on hydrogen and oxygen.

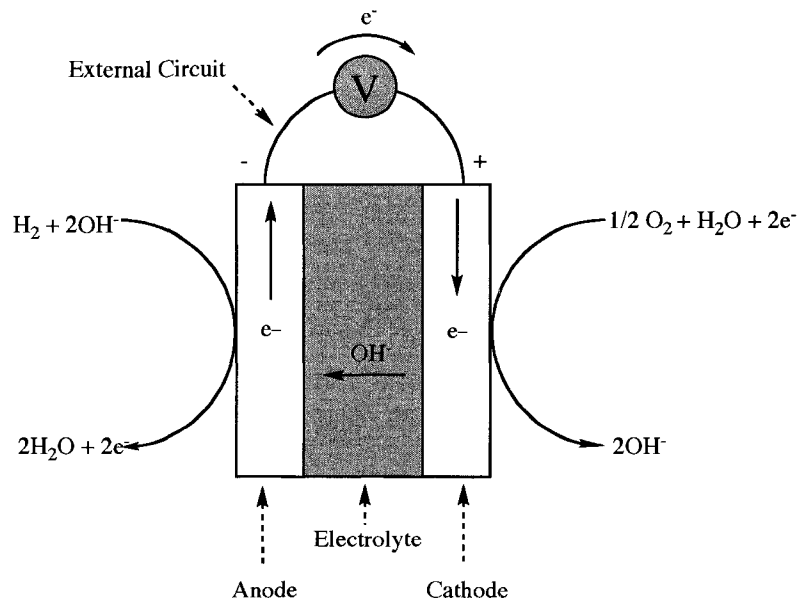


Figure 1-2: Schematic of an alkaline fuel cell.

The gases must be carefully scrubbed prior to use to prevent contamination by CO₂, which poisons the electrolyte by reacting to form carbonates.²⁸ These carbonates poison the electrodes and inhibit ion migrations thus decreasing the overall efficiency of the cell and requiring the contaminated electrolyte to be replaced often.¹⁷

Phosphoric Acid Fuel Cells (PAFCs):^{29,30} These cells operate at mid-range temperatures between 150°C and 220°C. The electrolyte consists of concentrated phosphoric acid, which is stable at these temperatures. PAFCs have better anode kinetics than PEMFCs due to their higher operating temperatures. Further, CO poisoning is less severe, so less pure hydrogen sources can be used.^{20,21} The heat from the steam formed at the cathode can be recovered, thus increasing the overall efficiency of the cell.²¹ For example, the Northern Alberta Institute for Technology in Edmonton, AB operates a 200 kW PAFC on their campus.³¹ A reformer station on site reforms methane to form H₂ and CO₂, which are fed into the cell and converted directly to electricity however, the fuel cell stack has to be replaced about every 40 000 h, or 5 years, because of loss of activity due to sintering.³⁰ Additional disadvantages are that the highly caustic electrolyte necessitates corrosion prevention technology and PAFCs experience long-term performance degradation.²⁹

Molten Carbonate Fuel Cells (MCFCs):^{32,33} These high temperature, 600°C-700°C, fuel cells employ molten (liquid) carbonate salts of lithium, potassium, or sodium as the electrolyte. During operation of a MCFC, carbonate ions migrate from the cathode to the anode where they combine with hydrogen to produce carbon dioxide, water, and electrons. The electrons travel back through an external circuit to the cathode where they react with oxygen and carbon dioxide to produce carbonate. The advantages of MCFCs are that the

high operating temperatures increase reaction kinetics and the cells typically have efficiencies near 60%.³² The efficiencies of these systems are increased to nearly 80% if the waste heat is used.³² MCFCs are less prone to CO poisoning than other types of fuel cells and so a wider range of fuels can be used compared to PEMFC.³³ The disadvantages are the need to inject carbon dioxide into the cathode to replenish the carbonates, and the structural corrosion that occurs at high temperatures.²⁰ MCFCs are best suited for large-scale stationary industrial applications for the production of heat and electricity.³³

Solid Oxide Fuel Cells (SOFCs):^{34,35} SOFCs are high temperature fuel cells that operate between 800°C and 1000°C. At the cathode, oxygen (from air) is reduced to form O^{2-} , the charge carrier, which travels from the cathode to the anode through a solid ceramic electrolyte (often zirconium oxide stabilized with yttrium oxide). At the anode, the fuel (H_2 , CO, CH_4 , etc.) is oxidized to form H_2O or CO_2 , (or both) and electrons. The electrons travel through an external circuit back to the cathode. SOFCs do not require precious metal electrocatalysts due to the faster reaction kinetics associated with the high operating temperature.²¹ Additionally, the high operating temperatures allow for fuels such as natural gas to be processed internally, and SOFCs regularly have efficiencies greater than 60%.³⁴ Some disadvantages for the adoption of SOFCs for widespread use are the large manufacturing and maintenance

costs associated with the high temperature corrosion of the cell materials and the smaller reversible potentials compared to lower-temperature fuel cells.²⁰ It should also be noted that, at these high operating temperatures, the Carnot advantage of SOFCs over ICEs is less because the Carnot efficiency at high temperatures nears 100%. Take, for example, a steam turbine operating at 1000°C (1273°K), the theoretical efficiency of such a system is 76.6%.

$$\eta = \frac{T_1 - T_2}{T_1} = \frac{1273 - 298}{1273} = 76.6\% \quad \text{Eq. 1-9}$$

SOFCs are most commonly used to produce heat and electricity in stationary industrial uses, though select vehicle uses exist.³⁵

Table 1-1. Summary and comparison of the major types of fuel cell.²²

	PEMFC	AFC	PAFC	MCFC	SOFC
Operating Temperature (°C)	50-125	60-90	150-220	600-700	800-1000
Electrolyte	Ion Exchange Membrane	Potassium Hydroxide	Phosphoric Acid	Molten Carbonate	Ceramic ZrO ₂ -Y ₂ O ₃
Fuel	H ₂	H ₂	H ₂	H ₂ , CO, etc.	H ₂ , CO, CH ₄ , CH ₃ OH, etc..
Anode Catalyst	Pt/C, PtRu/C	Pt/C	Pt/C	Ni-Cr/Ni-Al	Ni/ZrO ₂
Cathode Catalyst	Pt/C	Pt/C	Pt/C	Lithiated NiO	Sr-doped LaMnO ₃
Charge Carrier	H ⁺	OH ⁻	H ⁺	CO ₃ ²⁻	O ²⁻
Typical Efficiency	40-60%	50-60%	55%	55-65%	55-65%

1.3 Direct Methanol Fuel Cells (DMFCs):^{20,36,37} DMFCs are a type of PEMFC that use liquid methanol as a fuel rather than hydrogen gas. The cell is composed of a solid, acidic membrane electrolyte capable of conducting ions (most often Nafion[®]) and noble metal electro-catalysts at both the anode and cathode. Methanol is fed directly to the anode where it is electro-oxidized to CO₂, protons and electrons. The protons migrate from the anode to the cathode (ionic conduction), while the electrons travel in the same direction through an external circuit. Figure 1-3 shows a simplified schematic of a direct methanol fuel cell.

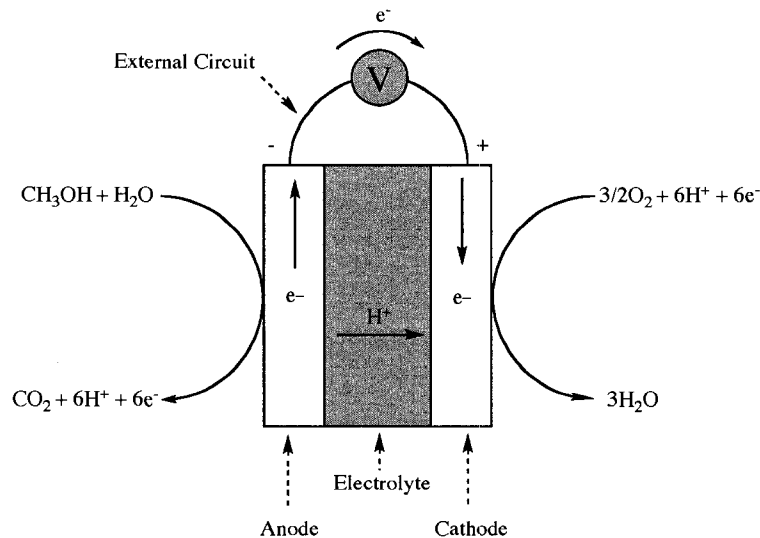


Figure 1-3: Schematic of a direct methanol fuel cell.

The half-cell reactions and overall cell reaction are shown below:





DMFCs operate at temperatures between 60°C and 130°C and have typical efficiencies near 40%.³⁸ Methanol shows promising activity compared to other alcohols and it is inexpensive. Methanol is a liquid at operating temperatures, and it can be used directly as the fuel, eliminating the need for in-cell reforming, and avoiding the problem of hydrogen storage. Additionally, methanol has a very high energy density compared to other fuels. Energy density is the amount of energy that can be produced from a unit mass or volume.

Recently, prototype DMFC cartridges for portable electronics such as laptops, cell phones and PDAs have become available. Internationally there are approximately 5500 portable DMFC units in use today, and portable units comprise of 75% of all installed DMFCs.³⁶ For example, MTI Micro Fuel Cell's Mobion[®] DMFC cartridge has demonstrated power of 50 mW cm⁻¹ and provides 1.4 Whr per cc of fuel.³⁹ While methanol is relatively non-toxic, it must be carefully handled and the cell design must prevent any leakage because of health and safety hazards associated with methanol ingestion.

Despite the advantages of DMFCs over other fuel cells, there are two large obstacles that must be overcome before the technology can be widely adopted in practical systems. One obstacle is that the electro-oxidation of

methanol suffers from sluggish kinetics that result from poisoning of electro-catalysts by strongly adsorbed intermediates such as carbon monoxide.²¹ High loadings of precious metal electro-catalysts, the most studied being Pt/Ru, are usually required to overcome these sluggish kinetics. The cost and loadings required are prohibitive and recently, the price of ruthenium has increased dramatically. Research and development in the area of catalyst improvement focuses on enhancing the preparation methods for Pt-Ru catalysts, preparing stable and highly dispersed carbon material supports for the catalysts, and exploring new catalysts materials that contain lower precious metal content in order to decrease costs.

Another obstacle faced by DMFCs is that methanol permeates through the Nafion[®] polymer electrolyte membranes, allowing methanol to cross over from the anode to the cathode.⁴⁰ Methanol crossover occurs in DMFCs because of diffusion and electroosmotic drag from protons migrating from the anode to the cathode. This crossover poisons the cathode, and it results in loss of methanol through evaporation. Methanol crossover is usually addressed by use of elaborate cell designs, controlled fuel feeding systems, alternative membrane materials, and high precious metal loadings at the cathode.⁴⁰ All of these approaches add to the cost and can limit the operational lifetime of the cell. Research specific to membrane design focuses on the use of a variety of polymers (random copolymers, graft copolymers, block copolymers, polymer blends) in addition to impregnated, coated and

composite membrane materials to limit methanol crossover without hindering proton conductivity.^{37,41}

Despite the recent advances in DMFC technology, the problems of methanol permeability and expensive precious metal electro-catalysts make it necessary to examine and develop alternative fuel cells.

1.4 Direct Alcohol Alkaline Fuel Cells (DAAFCs): Alkaline fuel cells have several advantages over acid-based cells. Perhaps the major advantage is that the kinetics for oxygen reduction are much faster than in acidic systems.⁴² Additionally, the kinetics for alcohol oxidation at the anode are also faster than in acidic systems.⁴² Another advantage of alkaline electrolytes is that a wider choice of metals is available for electro-catalysts because more metals, including inexpensive non-noble metals, are more stable to dissolution in alkaline than in acidic electrolytes.⁴³ Alkaline systems are also less corrosive than their acidic counterparts.

Direct alcohol alkaline fuel cells (DAAFCs) are promising alternatives to acid-based systems. In DAAFCs the hydroxide ion charge carrier is transported through the electrolyte from the cathode to the anode, opposite the direction of charge carrier flow in acid-based systems. This opposing charge carrier flow reduces alcohol crossover. Thereby, in principle, lower cathode loadings are required in DAAFCs. Several alcohols have been investigated for their suitability as a fuel. Methanol is the most studied of the alcohols because

of its relatively high activity and availability. The oxidation of methanol, however, produces carbon dioxide, which forms carbonates in alkaline media and greatly decreases the activity of the cell.

In a recent report, an alkaline DMFC equipped with an anion-exchange membrane, standard loadings of Pt/Ru and Pt electro-catalysts, operating on 1 M methanol and oxygen gas, obtained a power density of 16 mW cm^{-1} at 60°C . The power density decreased to 6 mW cm^{-1} at ambient conditions.⁴⁴ It was observed that cell performance increased with higher temperatures though increasing the methanol concentration had the effect of promoting crossover, which decreased the cell's performance. It should be noted however that the decrease in performance at higher methanol concentrations was less than those observed in acidic systems.⁴⁴

2-Propanol is potentially a highly suitable fuel for direct alcohol alkaline fuel cells. 2-Propanol is less toxic than methanol and cathode poisoning by 2-propanol is less severe than by methanol.^{45,46} Further, the main electrooxidation product at low potentials is acetone.⁴⁶ The electro-oxidation of 2-propanol to acetone does not involve strongly adsorbed intermediates and it does not produce CO_2 . For these reasons, the electro-oxidation of 2-propanol in an alkaline media poisons the anode less than methanol. Figure 1-4 shows the operation of a direct 2-propanol alkaline fuel cell:

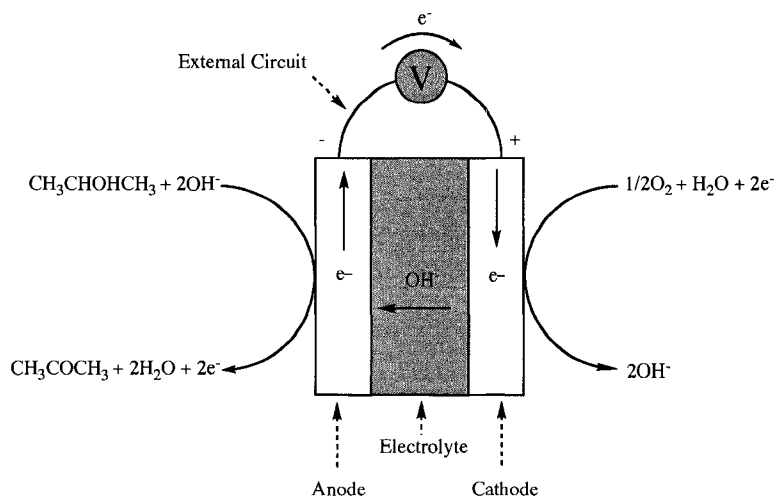
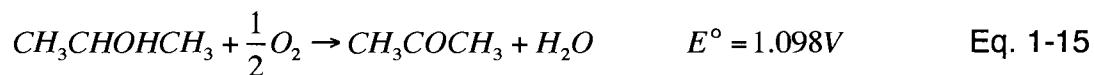
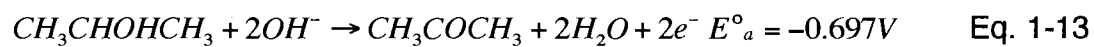


Figure 1-4: Schematic of a direct 2-propanol alkaline fuel cell.

At the cathode, oxygen is reduced to form hydroxide. The hydroxide (charge carrier) migrates through the electrolyte to the anode. At the anode, 2-propanol (fuel) is oxidized in the presence of hydroxide to form acetone, electrons and water. The electrons travel through the external circuit back to the cathode. The half-reactions and overall cell reactions are shown below:



The most important advantage of this type of fuel cells is that, since the partial oxidation of 2-propanol yields acetone it is, in principle, possible to regenerate the fuel by reducing the acetone back to 2-propanol. This regeneration can be accomplished electrochemically in the cell or by

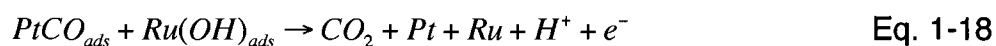
hydrogenation using an external catalyst.⁴⁷ The ΔG° for this reaction is 134.5 kJ mol⁻¹.⁴⁸ Additionally, the oxidation of 2-propanol to acetone does not produce CO₂, eliminating the need for an anode exhaust, avoiding the formation of carbonates in alkaline electrolytes, and allowing for a fully sealed compartment. Such a system would constitute a significant breakthrough in the field of alternate energy.

Methanol, on the other hand, is not regenerative and its oxidation leads to the formation of CO₂. Interestingly, 2-propanol is sometimes discounted as a fuel in favor of methanol because of its larger size and lower energy density. To better understand of relative similarity of these two fuels let us take, for example, the energy stored in a 15 inch, 900 g, Li-ion MacBook Pro[®] battery. The specifications indicate that such a battery is rated at 60 W hrs at 10.8 V. This power density corresponds to running a current of 5.6 A at 10.8 V for 1 hr, equivalent to 0.21 moles of electrons. This specification would only require a total of 6.3 g of 2-propanol being converted to acetone or 1.7 g of a 1:1 methanol:water mixture being completely converted to CO₂. As the cell components for systems running on methanol or 2-propanol would inherently be identical, it is, in our opinion, nonsensical to discount 2-propanol from contention as a suitable fuel.

Most research surrounding direct 2-propanol fuel cells has been undertaken in acidic systems where higher currents at lower potentials are produced than in methanol fuel cells. For example, the open circuit voltage of

a fuel cell operating on 2-propanol fuel cell is approximately 220 mV greater than the same cell when operating on methanol.⁴⁵ This difference in cell potential is maintained up to current densities of approximately 200 mA cm⁻².⁴⁵ At higher current densities there is a rapid decrease in the 2-propanol cell voltage due to poisoning of the anode. The higher currents at low potentials result from the electrooxidation of 2-propanol to acetone without the formation of a strongly adsorbed intermediate such as the CO. At low anode potentials the main electro-oxidation product is acetone but at higher potentials CO₂ forms accompanied by a decrease in current, which proceeds through a strongly adsorbed intermediate. Our research group recently investigated the electrooxidation of 2-propanol in base in order to further increase the current at low anode potentials and to widen the window between the onset of the electro-oxidation to form acetone and the electrooxidation to form CO₂.⁴⁶ Indeed, currents for the potentiostatic electrooxidation of 2-propanol over platinum were higher at low potential in base than in acid. In fact, a substantive current maximum was observed at low potentials for the potentiostatic oxidation of 2-propanol over platinum in base. To the best of our knowledge this system produced the highest normalized current to date for any alcohol/ electrocatalyst combination at low potentials required to achieve high efficiencies in direct alcohol fuel cells.

1.5 Summary and Research Proposal: The most commonly used anode electrocatalysts for PEMFCs, DMFCs, and DAAFCs are Pt/Ru nanoparticles supported on carbon.⁴⁹ Alone, platinum is easily poisoned by CO (*vide supra*). Oxides of ruthenium, when located in close proximity to the platinum, promote the oxidation of CO to CO₂ and thus help to protect and maintain the activity of the platinum surface. The processes by which ruthenium promotes the oxidation of CO to CO₂ are ascribed to electronic (ligand) effects and to the bifunctional mechanism.⁵⁰ The bifunctional mechanism for an acidic DMFC system is illustrated below:



Essentially, ruthenium forms oxides at low potentials. These oxides oxidize the CO on platinum. The high cost of Pt/Ru electro-catalysts are prohibitive to the development of commercially available fuel cells units. Much PEMFC/ DMFC/ DAAFC research focuses on the development of new anode electrocatalysts that are of less expensive metals and more active than Pt/Ru. The goal of the research described in this dissertation is to develop low loading Pt-Ni electrocatalyst systems for the electrooxidation of 2-propanol in alkaline electrolytes.

Several groups have reported on the activity of electrocatalysts containing platinum and nickel to develop alternatives to Pt/Ru anodes in

DMFC systems. Nickel is a desirable co-catalyst metal because it is inexpensive, abundant and stable to dissolution in alkaline electrolytes. Antolini et al.⁵¹ reported a commercially available, carbon supported Pt-Ni alloy electrocatalyst. The atomic composition of their catalyst was established via EDX analysis and the Ni content of the samples varied between 7-34 at.%. The alloy electrocatalysts had poor homogeneity and a poor degree of alloying. The Pt-Ni/C electrode was compared to Pt/C from the same supplier. The comparisons were made in a 2 M CH₃OH cell operating at 70°C and 90°C at oxygen pressures of 1 atm and 3 atm, respectively. The authors reported that the Pt-Ni/C had a greater maximum power density than Pt/C when operating as a cathode for the oxygen reduction reaction (ORR), and that the cell performance with the Pt-Ni/C cathode was superior than that with the Pt/C cathode. When the Pt-Ni/C electro-catalyst was in the anode of a fuel cell, the cell performance was comparable to Pt/C.

In another paper, Antolini et al.⁵² prepared Pt-Ni electrocatalysts with nominal atomic ratios of 90:10 and 70:30 via low-temperature borohydride reduction onto high surface area carbon. The atomic ratios of the electrocatalysts were again characterized by EDX and the actual compositions were near the nominal compositions. The Pt-Ni/C electrocatalyst were examined as anodes for the methanol oxidation reaction and as cathodes for the oxygen reduction reaction and compared to a commercially available carbon-supported platinum catalyst. In accordance with the results reported above,

the performances of the fuel cell using Pt-Ni/C as cathodes was superior to a cell using Pt/C as a cathode (2 M CH₃OH at an O₂ pressure 0.3 Mpa and at 90°C). The performance of the Pt-Ni/C cathode depended on the amount of alloyed nickel, not the total amount of nickel present in the composite. It was also reported that a low degree of alloying leads to better performance as an anode material.

Mathiyarasu et al.⁵³ electrochemically deposited films of Ni and Pt onto a gold surface. The atomic compositions of the deposits were controlled by varying the concentration of nickel in the plating bath. The approximate ratio of Pt to Ni was determined by XRF-EDX and the four prepared Pt/Ni electrodes had nickel contents between 4 and 10 at.%. The Pt/Ni electrodes were compared to Pt for the methanol oxidation reaction (MOR) in a standard 3-electrode cell containing a 0.5 M H₂SO₄/ 0.5 M CH₃OH electrolyte. It was reported that the Pt/Ni anodes produced larger polarization currents than the Pt anodes and that the onset potential for methanol oxidation was lower. Additionally, the stabilized current after 1 hr was 3 orders of magnitude greater using an electrode containing 8 at.% Ni than using a pure Pt anode.

Drillet et al.⁵⁴ prepared a Pt/Ni disk electrode by melting 7 equivalents of Pt pellets and 3 equivalents of Ni pellets in a vacuum arc oven. The atomic ratio of Pt and Ni on the electrode surface was determined before and after each experiment using XPS. In a standard 3-electrode cell containing oxygenated 1 M H₂SO₄, the Pt/Ni disk electrode was compared to a Pt disk

electrode for the oxygen reduction reaction. The onset of electrode oxidation was higher, and the overpotential for oxygen evolution was lower with Pt/Ni electrode. The Pt/Ni was also a more methanol-tolerant cathode.

Yang et al.⁵⁵ prepared carbon supported Pt/Ni alloy nanoparticles using a carbonyl complex and high temperature H₂ reduction. Analysis with EDX showed that the nickel content for 4 prepared electrodes ranged between 32.9 and 45.4 at.%. The authors compared the Pt/Ni electrocatalysts to a commercially available carbon supported Pt electrocatalyst for the ORR. Using a standard 3-electrode cell with an oxygenated 0.5 M H₂SO₄ electrolyte the authors reported that the Pt/Ni alloys were more active to the oxygen reduction reaction. Additionally, the open circuit potentials of the Pt/Ni electrocatalysts were higher than that of a Pt/C electrocatalyst. The authors also report that this Pt/Ni alloy is more tolerant to methanol than Pt/C.

Colón-Mercado et al.⁵⁶ used a commercially available carbon-supported Pt/Ni electrocatalyst and compared its activity and long-term durability for the oxygen reduction reaction to a carbon-supported platinum electrocatalyst. The Pt/Ni electrocatalysts were used as received. The comparisons were made using a standard 3-electrode cell with 0.3 M H₂SO₄. The authors reported that the Pt/Ni alloy was more resistant to sintering and that a strong correlation exists between the activity towards oxygen reduction and the amount of nickel dissolved from the electrocatalyst.

Stamenkovic et al.⁵⁷ prepared two Pt/Ni alloy surfaces by sputtering and annealing. The two surfaces were characterized by low energy ion scattering spectroscopy (LEISS). The sputtered surface contained 25% nickel, and the annealed surface displayed characteristics of surface segregation leading to a pure platinum “skin”. The Pt/Ni alloys were more active than Pt towards the oxygen reduction reaction over a range of temperatures in 1 M HClO₄. The activity of the annealed surface was greater than the sputtered surface.

Rahim et al.⁵⁸ prepared graphite supported Pt/Ni nano-particles via the electrochemical codeposition of platinum and nickel salts. The size of the nano-particles was determined using SEM and the compositions were determined using EDX. The methanol oxidation activity of the Pt/Ni electrodes was compared to a graphite supported Pt electrode prepared by the same method. The Pt/Ni electrodes were more active than Pt towards the methanol oxidation reaction in 1 M KOH. The Pt/Ni electrodes showed were more stable than Pt, and the catalytic activity depended on the content of nickel, with 5% nickel providing the greatest activity.

Pt/Ni electrocatalysts prepared from macrocycle precursors were more active towards methanol oxidation than pure platinum, in particular after heat-treatment.^{59,60} Unsupported Pt/Ni electrocatalysts prepared by borohydride reduction of metal salts were tested in 3-electrode cells^{61,62,63} and in fuel cells^{61,62} under acidic conditions and also showed greater activity towards the oxidation of methanol than platinum. Pt/Ni electrocatalysts prepared by

sputtering⁶⁴ and electron-beam evaporation,⁶⁵ tested in 3-electrode cells were found to be better cathode material for the oxygen reduction reaction than platinum in the presence of propanol. Nickel has been found to be stable in Nafion^{®59} and it has been shown that the platinum lattice helps to stabilize nickel in acidic media.^{53,56,66}

As discussed above, it has been shown that the presence of nickel in Pt or Pt/Ru electro-catalysts increases the catalytic activity of platinum towards methanol oxidation and the oxygen reduction reactions. Means by which nickel increases the activity of the electrocatalysts include the bi-functional mechanism (*vide supra*) and electronic (ligand) effects.^{53,54,56,58,61,63,67} Parallel to ruthenium, nickel is an oxophilic metal that produces surface oxides. At low potentials a monolayer of weakly bonded Ni(OH)₂ forms and at higher potentials the formation of NiOOH occurs. The oxides of nickel promote the oxidation of adsorbed CO, forming CO₂. The presence of nickel as a co-catalyst also decreases the binding energy of platinum and weakens the Pt-CO bond, thus decreasing poisoning of the catalyst surface.^{62,63}

1.6 Conclusion: To the best of our knowledge, no group has yet examined the activity of binary Ni/Pt electrocatalysts towards the oxidation of 2-propanol in alkaline electrolytes. We therefore produced a Ni/Pt anode material that can generate reasonably high currents using 2-propanol as a fuel, but requires only a fraction of the standard loading of platinum metal. The preparation of a

low Pt loading, active Ni/Pt electrocatalyst via an evolving electrochemical co-deposition for use in an alkaline 2-propanol fuel cell is described. The activity of this electrode material is compared to pure platinum, pure nickel and a second type of Ni/Pt electrode prepared via co-deposition of metal salts.

Chapter 2: Ni/Pt Anode Materials for the Electrooxidation of 2-Propanol in Alkaline Electrolytes

2.1 Electrodeposition of Anode Materials: Blacked platinum gauzes (Pt_{Black}) were prepared following standard literature procedure.⁶⁸ The cyclic voltammograms of the resulting gauzes were characteristic of blacked platinum electrodes.⁶⁹ The cyclic voltammograms were used, when necessary, to measure the specific surface area of the electrodes. These Pt_{Black} electrodes were used for two purposes: as an anode material for comparison of the electrochemical activity towards 2-propanol oxidation, and as the counter electrode for the majority of the electrochemical analyses. All potentials are reported versus the standard hydrogen electrode (SHE), unless otherwise stated.

In order to carry out the deposition of Pt onto the electrode surfaces, we required blacked nickel gauzes because they provided quantifiable and high surface area supports. Blacked nickel electrodes (Ni_{Black}) were prepared following a procedure based on the work of Marozzi et al.⁷⁰ In their work, the authors prepared highly porous, mechanically-stable nickel electrodeposits for use as electrode materials. Deposition solutions consisting of 0.2 M NiCl_2 in 0.25 M to 4 M NH_4Cl were galvanostatically electrodeposited onto supports at current densities ranging between -0.03 A cm^{-2} and -5 A cm^{-2} . The authors found that the presence of NH_4Cl in the electrolyte enhanced the mechanical

stability of the deposit. The mechanism by which NH_4^+ increases mechanical stability is by preventing the formation of $\text{Ni}(\text{OH})_2$ at low current densities by favoring the formation of complex compounds such as $\text{Ni}(\text{NH}_3)_n^{2+}$ instead. Additionally, increasing the NH_4Cl concentration in the deposition bath increased the range of current densities over which strongly adhered and mechanically stable deposits were obtained. At NH_4Cl concentrations of 2.0 M, current densities as high as -0.5 A cm^{-2} were found to produce deposits with strong mechanical stability and the authors reported that the surface area of the electrodeposits varied with the applied current. Current densities of -0.1 A cm^{-2} gave stable, relatively high surface area systems. Based on those observations, we chose to prepare our blacked nickel electrodes by galvanostatically depositing at -0.1 A cm^{-2} from a deposition bath consisting of 0.2 M NiCl_2 / 2.0 M NH_4Cl .

For our preliminary investigation, we used a blacked Pt gauze as our counter electrode. The Pt_{Black} electrode was in the same electrolyte as the working electrode and not isolated behind a frit. The resulting deposition behavior was unexpected. Figure 2-4 shows the potential of the working electrode as a function of time during the electrodeposition.

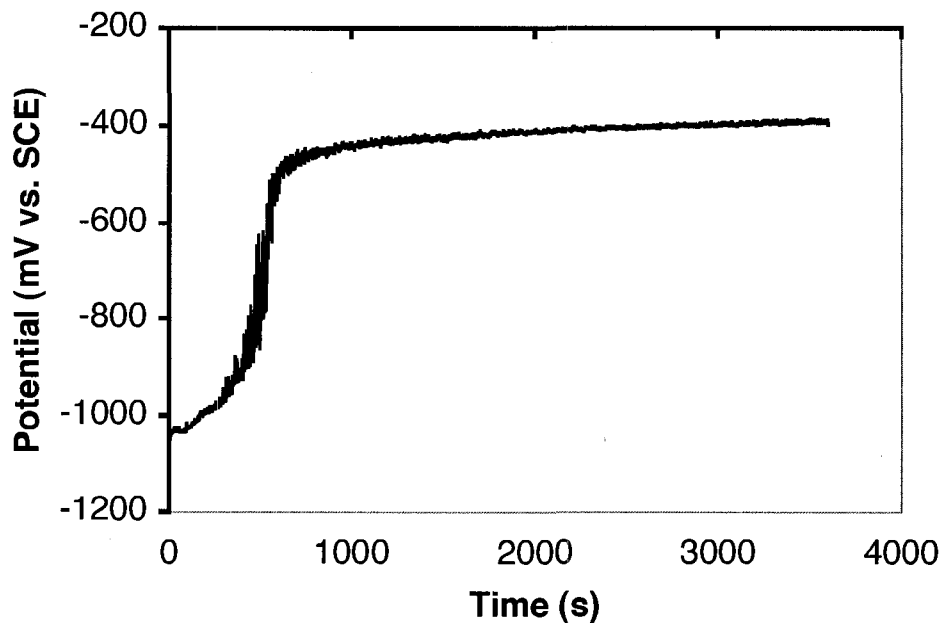


Figure 2-1: Deposition potential of the working electrode over time during blacking at -0.1 A from 0.2 M NiCl_2 / 2.0 M NH_4Cl .

As the current was applied to the working electrode, the potential quickly dropped from open circuit potential down to -1050 mV vs. SCE. After a short period of polarization, there occurred a significant, dramatic increase in potential over the first 500 seconds until the potential stabilized near -400 mV vs. SCE. Significant H_2 evolution was observed at the working electrode when the potential began to stabilize. The potential behavior and the production of gas at low potentials clearly indicated that a significant change in the surface composition of the electrode had occurred. We believed that this behavior was due to platinum contamination from the counter electrode, because nickel does not lead to the formation of hydrogen at these potentials.

To test this hypothesis, we performed the same deposition using a graphite counter electrode. In this case, the potential versus time behavior of the electrode was as expected. Specifically, when the current was applied to the working electrode, the potential quickly dropped from open circuit potential to -1050 mV vs. SCE. After this, the electrode potential stabilized near -1000 mV vs. SCE for the remainder of the hour. We expected a stabilized potential because the only reaction that should have been occurring was the reduction of Ni^{2+} onto the working electrode. The potential versus time behavior for the deposition of a Ni_{Black} electrode is shown in Figure 2-2.

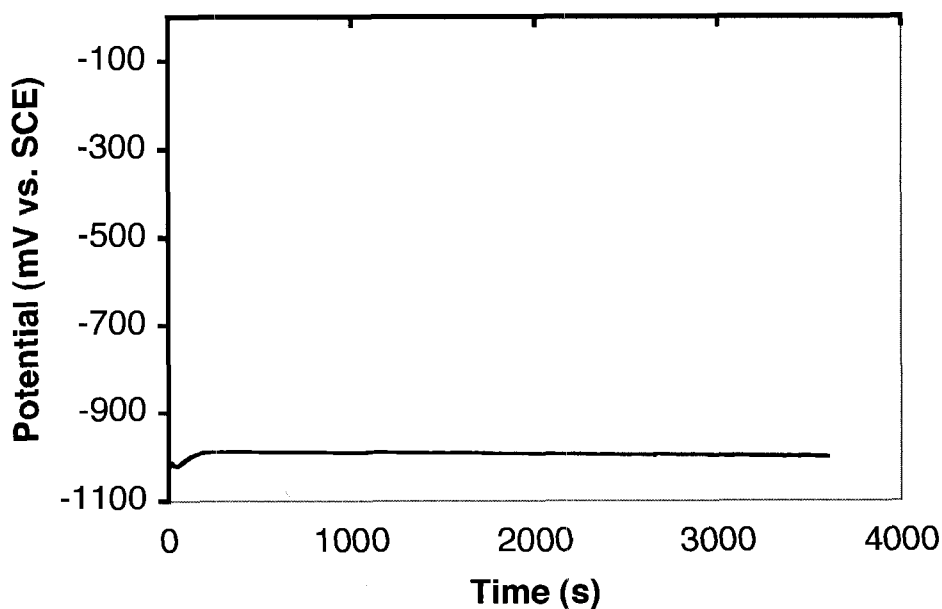


Figure 2-2: Deposition potential of an electrode over time, using a graphite counter electrode, during blacking at -0.1 A from 0.2 M NiCl_2 / 2.0 M NH_4Cl .

We were surprised to find that the characteristics of the resulting deposit depended on the nature of the counter electrode. Usually the use of a platinum counter electrode in the same electrolyte does not result in significant incorporation of platinum into the working electrode, which is not the case in these depositions. This finding is reminiscent of Rosenberg's discovery of a platinum anticancer complex from the electrolysis product of a platinum electrode.⁷¹

Platinum is known to dissolve in acidic chloride solutions.⁷² The dissolution is facilitated by the formation of platinum chlorides. Yadav et al.⁷³ reported that, when a platinum electrode was cycled from 0 to 1.4 V vs. SHE at a scan rate of 40 mV s⁻¹ and in an acidic electrolyte with chloride concentrations as low as 10 ppm. UV spectrums of the electrolyzed solution revealed the formation of platinum in both the Pt⁴⁺ and Pt²⁺ oxidation states, existing as PtCl₆²⁻ and PtCl₄²⁻ respectively. Platinum dissolution has been reported to occur in operating PEMFC's, leading to decreased cell voltages, reduction in cathode surface areas and platinum deposition at the membranes.^{74,75} This degradation begins at high electrode potentials and commences with the chemical dissolution of platinum oxides.^{75,76} Another possibility is that the platinum exists as an NH₃ compound.

Our discovery of a potentially low platinum loading system during the deposition process of blacked nickel gauzes shifted our focus and enticed us to examine the present system in further detail. We decided to investigate this

phenomenon to see if low loadings of platinum were being deposited, and if the resulting electrodes were active as electrocatalysts for the oxidation of alcohols.

To better understand this system, we focused our attention on investigating the role platinum plays during the deposition. Specifically, we wished to understand what processes facilitated the incorporation of platinum into solution and to quantify the amount of platinum being deposited. These electrodes will be referred to as Ni/Pt electrodes for the remainder of this dissertation.

2.2 Ni/Pt Anodes: The deposition of a Ni/Pt electrode was performed as described in Section 2.1. The potential of the Pt_{Black} counter electrode was recorded as a function of time during the deposition. Figure 2-3 shows that the potential immediately jumped from an open circuit potential of ~ 270 mV up to 740 mV. After ~ 90 seconds the potential of the counter electrode stabilized at 1147 mV (± 5 mV). The blips in potential are due to disturbance of the electrode as aliquots were taken.

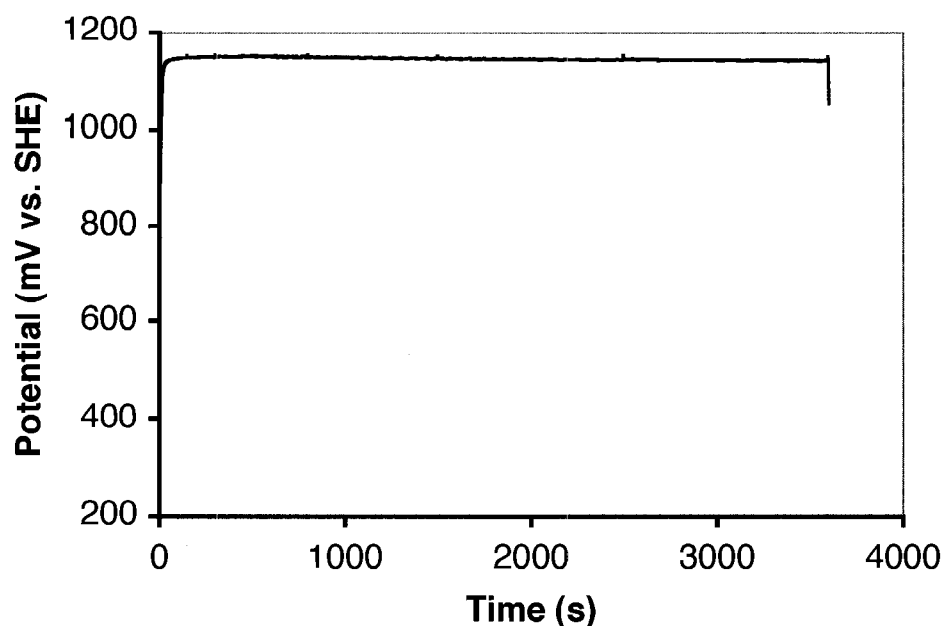


Figure 2-3: Deposition potential of the Pt counter electrode over time during the deposition of a Ni/Pt electrode.

The oxidation of Pt to Pt^{2+} occurs at 1.188 V vs. NHE under standard conditions. While the potential of the counter electrode did not reach 1.188 V, Yadev et al. observed that the formation of platinum-chloride complexes occurred at potentials as low as 1.06 V in acidic chloride electrolytes.⁷³

In order to quantify the amount of platinum present in solution, aliquots were taken from the bath at specified times and analyzed by ICP. Figure 2-4 shows the potential versus time behavior of a Ni/Pt electrode and the corresponding concentration of Pt in the bath as a function of time. The concentration of platinum peaks after the first 100 seconds and then decays quasi-exponentially over the remaining hour. The position of this platinum

concentration peak corresponds to the time period over which the potential of counter electrode increased and stabilized.

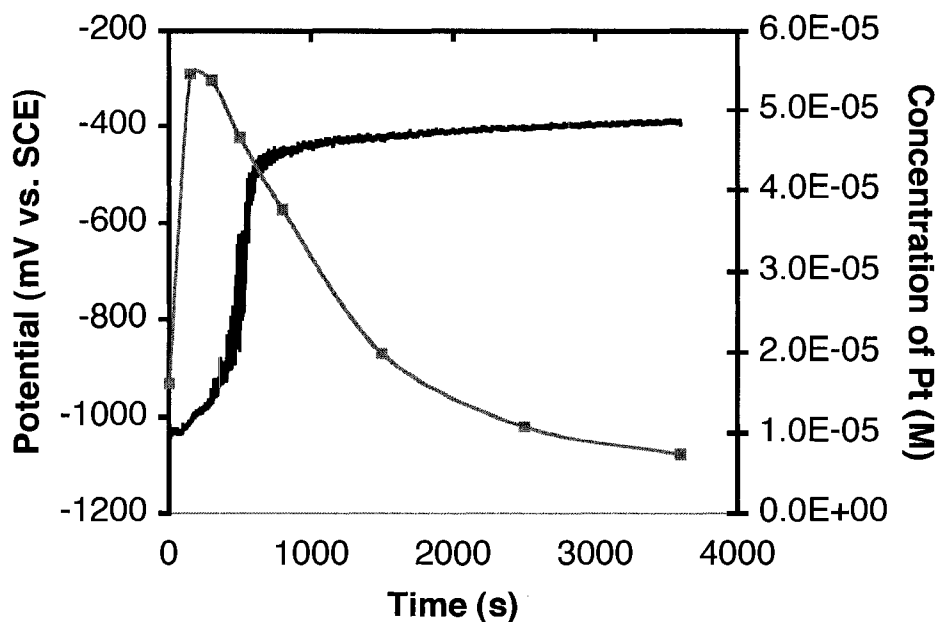


Figure 2-4: Potential behavior of a Ni/Pt Electrode (solid line) showing the concentration of platinum in the deposition solution as a function of time (squares).

Hydrogen evolution over nickel occurs near -1150 mV vs. SCE, while over platinum it is near -340 mV vs. SCE. These potentials were calculated from our experiments in base by observing the potential at which the cathodic current decreased dramatically and gas evolution was initiated, and we expected a similar difference to occur in the deposition bath. The deposition of Ni/Pt electrodes is accompanied by the production of a large quantity of H_2 after the first 500 seconds of potential stabilization. A constant current was drawn during the deposition and so the potential recorded for the working

electrode represented the process requiring the least potential. As the concentration of platinum in solution decreased, the amount of platinum deposited onto the electrode surface must then have increased. As this platinum was deposited, the current was directed towards the reduction of protons to form hydrogen rather than towards the reduction of Ni^{2+} . For this reason, we expected the total mass of the electrodeposit to be less than those obtained in the absence of platinum.

The mass of each electrode was determined prior to and after the electrochemical analyses. Figure 2-5 shows the average mass increases of Ni_{Black} and Ni/Pt electrodes. All of the electrodes were similar in initial size, so this increase is representative.

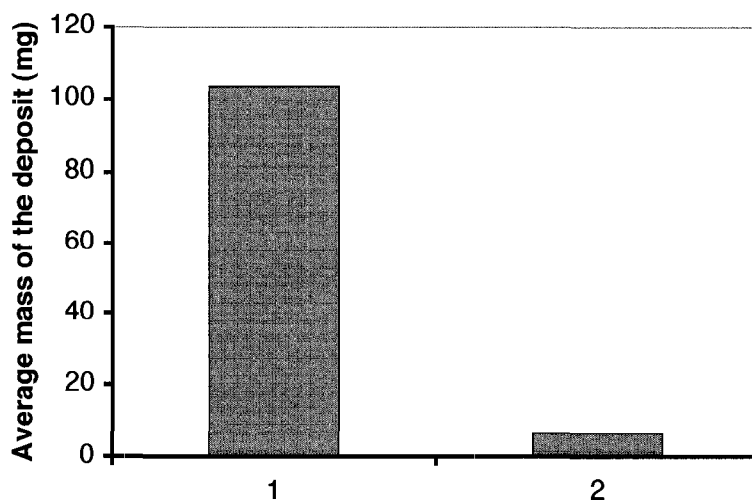


Figure 2-5: Average mass deposited onto (1) Ni_{Black} electrodes and (2) Ni/Pt electrodes.

These results show that the presence of platinum in the deposition solution, and therefore the presence of platinum on the surface of the electrode, does indeed decrease the total mass deposited by a large amount. The deposition is therefore, to some extent, self-regulating. Specifically, as the amount of platinum on the electrode surface increases, hydrogen production also increases. Increased hydrogen production decreases the degree of nickel and platinum deposition onto the electrode surface. The average mass increase of Ni/Pt electrodes was only 6.5 mg compared to the 103.4 mg gained, on average, by Ni_{Black} electrodes. This difference is significant and clearly demonstrated that platinum inhibited the deposition of nickel onto the electrode.

The preference for platinum deposition over nickel deposition is explained by their respective standard reduction potentials. The standard reduction potentials for Ni²⁺ to Ni and Pt²⁺ to Pt are -0.257 V and 1.180 V, respectively. Thus Pt²⁺ ions were deposited preferentially over Ni as the concentration of Pt²⁺ increased during the early stages of the deposition. Once these Pt²⁺ ions were deposited, hydrogen evolution began.

The total amount of platinum deposited was determined by ICP analysis. The electrodes were completely dissolved in hot aqua regia; the solution was then reduced to dryness, dissolved in 1% HNO₃, and analyzed by ICP. Figure 2-6 shows the average mass of platinum deposited onto the electrodes.

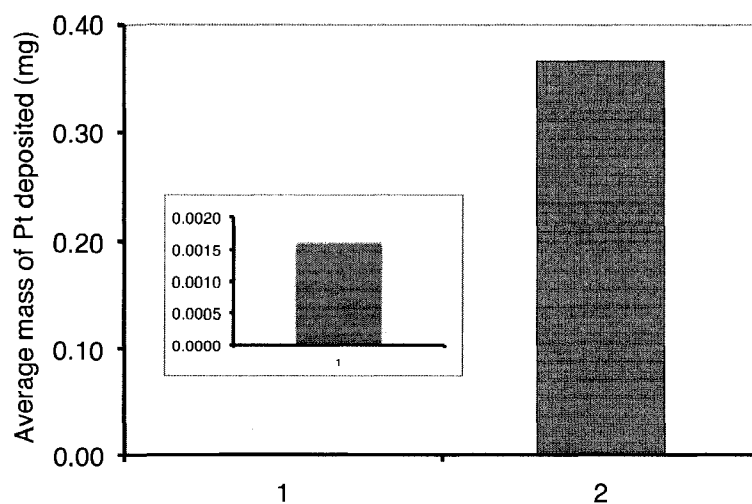


Figure 2-6: Average mass of Pt deposited onto (1) Ni_{Black} electrodes and (2) Ni/Pt electrodes.

Ni/Pt electrodes contain platinum. The Pt_{Black} counter electrode was not weighed before or after deposition, but its surface area before and after deposition was calculated from cyclic voltammograms taken in acid. These voltammograms showed a small decrease in the Pt_{Black} electrode's surface area following Ni/Pt electrode deposition. The average mass of platinum in the Ni/Pt deposit was 0.366 mg, indicating that the typical deposit was 5.6% Pt by weight, and it had an atomic composition of 1.8% Pt. We did not expect the Ni_{Black} electrodes to contain platinum but the ICP results showed that, on average, 0.0016 mg of platinum was present in the deposit. We believed this platinum to originate from impurities in the NiCl₂.

A simple yes/no qualitative test was applied to electrodeposited electrodes to confirm that platinum was at the surface of these electrodes. Platinum is known to catalyze the decomposition of H_2O_2 to release oxygen.



Figure 2-7: Decomposition of dilute H_2O_2 over a Ni_{Black} electrode, a Ni/Pt electrode and a Pt_{Black} electrode.

Figure 2-7 shows the degree of gas evolution over the three types of electrodes with varying degrees of surface platinum coverage. No gas evolution was observed over Ni_{Black} . Violent gas evolution was observed over Pt_{Black} . The Ni/Pt electrode produced a moderate gas evolution. This observation confirmed the conclusion drawn from the ICP results of the aliquot sampling during the deposition: platinum is present in the deposition solution and is being deposited onto the surface of the electrode.

2.3 Cyclic Voltammetry: Cyclic voltammograms were taken in 0.5 M NaOH. An alkaline electrolyte was used because we wished to replicate the conditions of an alkaline fuel cell and prevent the nickel dissolution known to

occur in acidic electrolytes. The cyclic voltammograms of both Pt_{Black} and Ni_{Black} were compared to those of Ni/Pt in the same electrolyte. All potentials are given versus the standard hydrogen electrode (SHE).

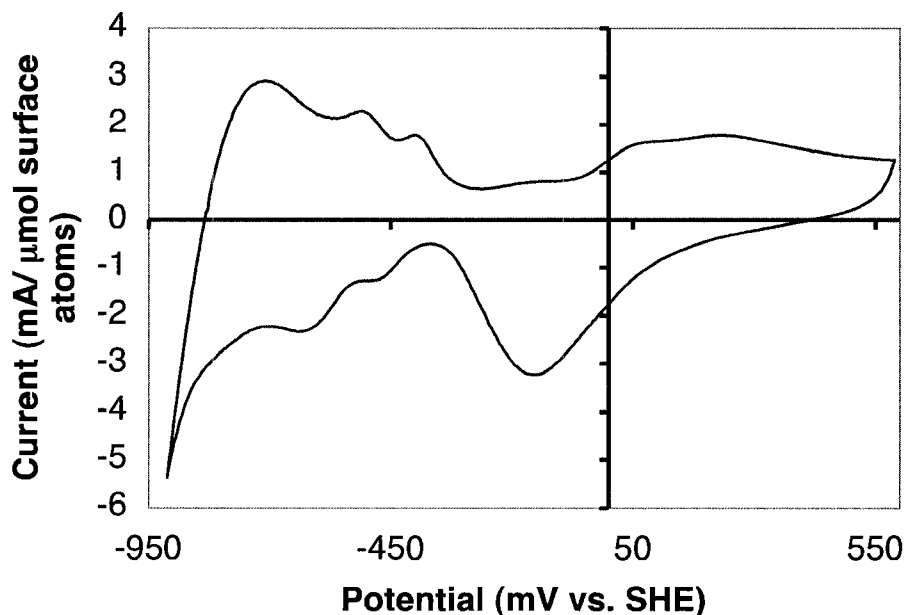


Figure 2-8: Cyclic voltammogram of a Pt_{Black} electrode in 0.5 M NaOH at a scan rate of 10 mV s⁻¹.

Figure 2-8 shows the cyclic voltammogram of a Pt_{Black} electrode in 0.5 M NaOH. Platinum electrodes have been extensively studied in both alkaline and acidic electrolytes.⁷⁷ The voltammograms can be divided into 3 distinct regions: the hydride region (-912 mV to -325 mV) where hydrogen is adsorbed and desorbed from the electrode surface, the double layer region (-325 mV to -40 mV), and the oxide region (-40 mV to 585 mV) where oxides of

platinum are formed and removed. This cyclic voltammogram is typical of

Pt_{Black}.

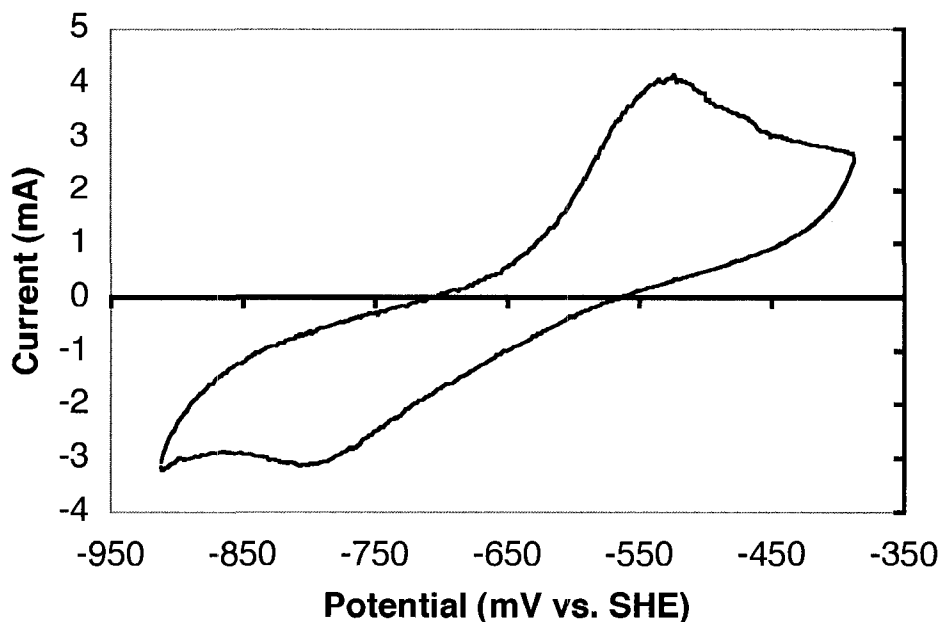


Figure 2-9: Cyclic voltammogram of a Ni_{Black} electrode in 0.5 M NaOH at a scan rate of 10 mV s⁻¹.

Figure 2-9 shows the stabilized cyclic voltammogram of a Ni_{Black} electrode in 0.5 M NaOH. The reactions and evolution of nickel in alkaline media have been studied extensively; Hahn et al.⁷⁸ provide a good review of the subject. Typical features include an anodic peak located at -540 mV corresponding to the oxidation of the nickel surface to form α -Ni(OH)₂. The reverse process can be observed with the cathodic sweep at -800 mV. This oxidation/ reduction process is fully reversible when the vertex potential of the

sweep is set negative of -380 mV.⁷⁹ At higher vertex potentials, multilayered β -Ni(OH)₂ forms, which is an irreversible process.⁷⁹

For the purpose of this research, all attempts were made to cap the potential maximum so as to prevent (or limit) the formation of β -Ni(OH)₂. Machado et al.⁸⁰ measured the anodic and cathodic charges obtained by cycling a nickel electrode in 0.5 M NaOH at 50 mV s⁻¹ from -1000 mV vs. SHE while increasing the upper potential limit with each sweep. They found that the potential limit at which the anodic charge became larger than the cathodic charge corresponded to the potential at which β -Ni(OH)₂ forms. This transformation was observed to occur at -380 mV vs. SHE. Limiting the potential sweep region to the formation and reduction of a monolayer of α -Ni(OH)₂ allowed for the determination of the real electroactive surface area of Ni_{Black} electrodes. Specifically, when the magnitude of the charges for the formation and reduction of α -Ni(OH)₂ were equal, the process was fully reversible and the surface area of blacked nickel electrodes could be calculated using the charge corresponding to one of the peaks.⁸⁰ We did not obtain peak charges of equal magnitude using the same potential range, however, our anodic and cathodic charges were within 10% and so we used this method used to approximate the surface areas for our Ni_{Black} electrodes.

Figure 2-10 shows the stabilized cyclic voltammogram of a Ni/Pt electrode in 0.5 M NaOH. As with Ni_{Black} electrodes, the upper sweep limit was kept negative of -380 mV to prevent (or limit) the formation of β -Ni(OH)₂.

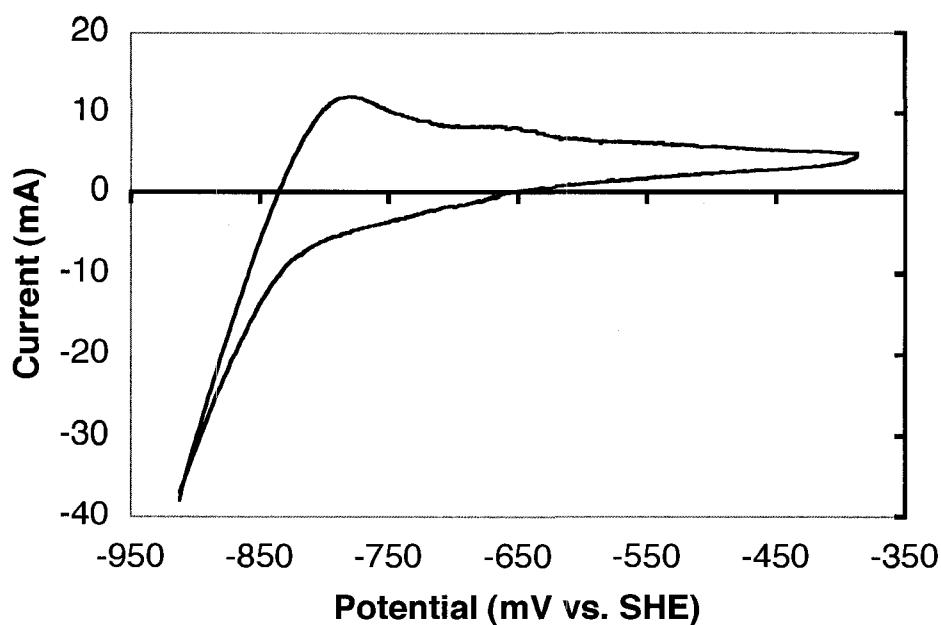


Figure 2-10: Cyclic voltammogram of a Ni/Pt electrode in 0.5 M NaOH at a scan rate of 10 mV s⁻¹.

Some characteristic platinum behavior was observed in the hydride region of the Ni/Pt voltammogram. Specifically, the sharp cathodic peak at -900 mV corresponded to the potential for hydrogen evolution, as was seen in the platinum cyclic voltammogram. Similarly, the anodic peaks at -775 mV and -650 mV were reminiscent of the hydride peaks characteristic of platinum. Peaks characteristic of nickel behavior were not observed. The most notable absence was that of the Ni(OH)₂ oxidation peak at -550 mV. As a result, the only similarity between the cyclic voltammograms of the Ni/Pt and Ni_{Black} electrodes was the net oxidation that occurred at potentials greater than -550 mV.

The observation of platinum character at low potentials and the lack of substantive nickel character in the Ni/Pt cyclic voltammogram indicated that the majority of the platinum deposited existed as surface platinum rather than residing in the bulk deposit. This conclusion was in agreement with the potential trends observed during the deposition process and with the observations made when the Ni/Pt electrodes were submerged in H_2O_2 .

2.4 CO Stripping Voltammetry: Carbon monoxide (CO) stripping voltammetry was used to try to quantify the amount of surface platinum on the electrodes. It is well established that the surface area of platinum electrodes can be estimated via this method.⁸¹ Carbon monoxide is potentiostatically adsorbed onto the electrode 50 mV and then oxidized off the surface by sweeping the potential. The charge of this peak relates to the specific surface area of the electrode.

CO stripping experiments were performed on Ni/Pt electrodes and Ni_{Black} electrodes. CO Stripping was done prior to the electrochemical experiments. Under these circumstances the stripping experiments were successful but, for reasons discussed below, the subsequent activity of the electrodes towards the oxidation of 2-propanol was greatly reduced. This occurs because the upper potential required to strip the CO resulted in nickel passivation and, likely, nickel and platinum dissolution. As a result, it was not

possible to perform both CO stripping and 2-propanol oxidation experiments on the same electrode.

Figure 2-11 shows the CO stripping voltammogram of a Ni_{Black} electrode in 0.5 M NaOH. CO adsorption was done by bubbling the gas through the electrolyte for 30 minutes while the potential was held at -1.2 V. The resulting voltammogram shows the presence of two oxidation peaks located at -505 mV and -285 mV respectively.

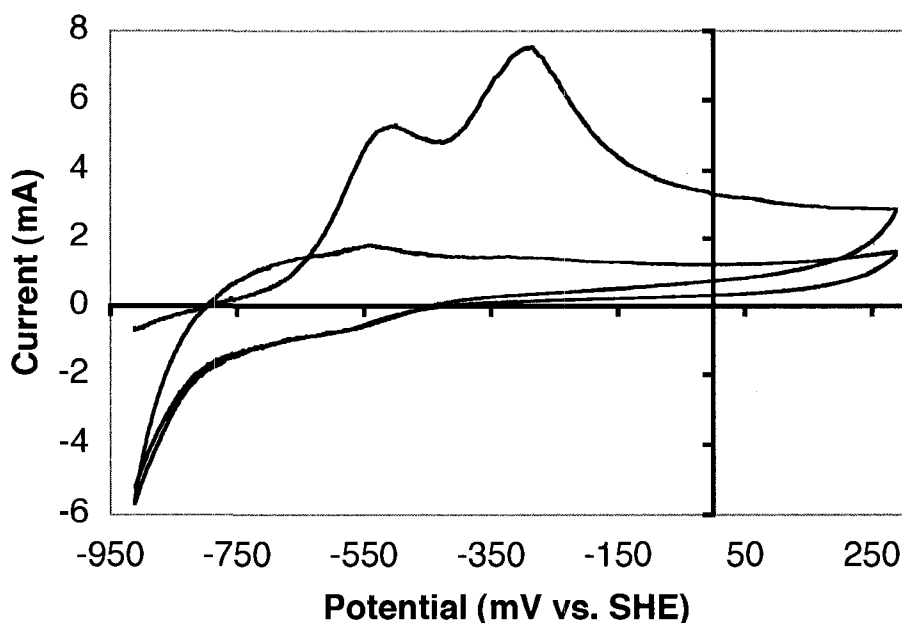


Figure 2-11: CO Stripping Voltammetry on a Ni_{Black} electrode in 0.5 M NaOH sweeping at 10mV s^{-1} for 2 sweeps.

The peak at -505 mV is present in the absence of CO, while the peak at -285 mV is absent under these conditions. This finding concurs with the cyclic voltammogram of a Ni_{Black} electrode shown in Figure 2-9, where the

oxidative peak for the formation of α -Ni(OH)₂ occurred near -520 mV. Thus the first peak in the CO stripping voltammogram is due to oxidation of Ni, and therefore the second peak is due to the oxidation of adsorbed CO. Carbon monoxide does not adsorb to all sites on the Ni electrode. In a similar experiment, Shervedani et al. also observed the presence of two CO oxidation peaks on porous Ni-Zn-P electrodes in alkaline electrolytes.⁸² They also believed that the first peak was primarily due to oxidation of the nickel surface and further explained that the first peak existed in the presence of CO likely because of pores in the surface too small for the CO to permeate. The surface area of Ni_{Black} electrodes studied here was calculated from the CO stripping data. The area of the first peak was calculated by taking a baseline from the linear portion of the first sweep from -900 mV to -750 mV. Assuming Gaussian behavior, half of the area of the curve was calculated by integrating to the peak maximum. The same technique was used for the second peak, but using the linear region of the curve from 200 mV to 225 mV as the baseline. Figure 2-12 is a visual representation of this process. For this electrode, the total area from the CO stripping voltammogram corresponded to a charge of 0.2053 C. The term "CO stripping charge" will be used to refer to the total charge obtained from both the peak corresponding to α -Ni(OH)₂ and to the peak corresponding to CO on nickel.

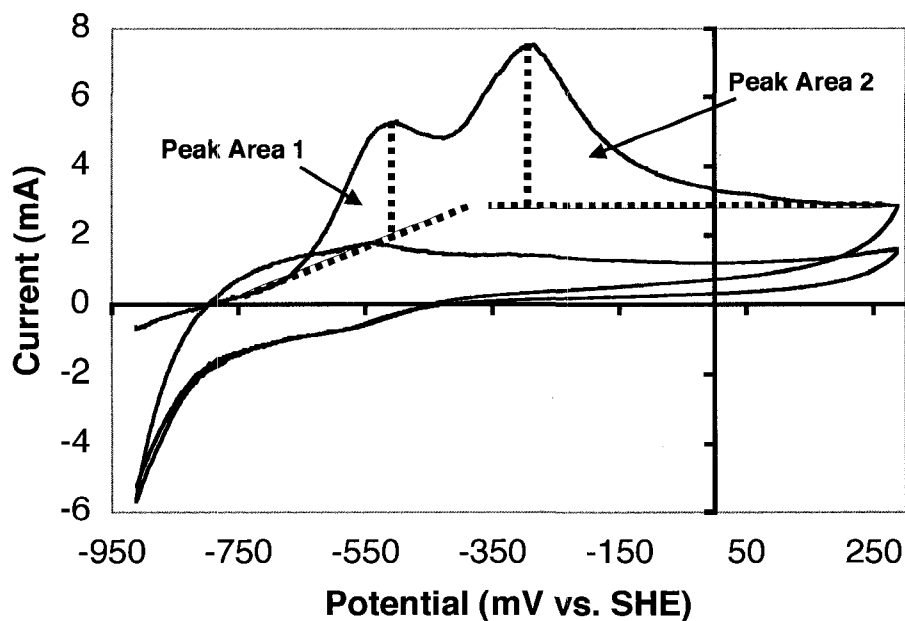


Figure 2-12: Illustration of the technique for calculating the CO stripping surface area of a Ni_{Black} electrode.

The area of this electrode was also calculated using the baseline cyclic voltammogram in the absence of CO, using the technique of Machado et al., as discussed in Section 2.3. From that analysis, the total area of the electrode corresponded to a charge of 0.08003 C, a value much smaller than the area calculated via CO stripping. We were also surprised to find that the peak in the CO stripping voltammogram attributed to the oxidation of Ni to α -Ni(OH)₂ at -505 mV had a charge nearly identical to the peak at the same potential in the baseline cyclic voltammogram. This finding leads us to conclude that the literature method used to calculate the area of nickel electrodes is an underestimation of the total surface area. We propose that not all of the surface nickel atoms are oxidized to form α -Ni(OH)₂ after sweeping in the

prescribed potential range (Section 2.3). Additionally, it appears that CO adsorption does not occur at the Ni sites that form α -Ni(OH)₂. Again, we believe this to be true because the area calculated for the first peak from the CO stripping voltammogram was approximately equal to the area calculated for the α -Ni(OH)₂ peak from its original cyclic voltammogram.

As a result of these findings, we propose a new method of better calculating the real surface area of nickel electrodes. The calculated charge for the formation of α -Ni(OH)₂ in the baseline cyclic voltammogram was 0.08003 C. The charge from the CO stripping voltammetry was 0.2053 C thus the CO stripping charge was 2.57 times greater than that for the formation of α -Ni(OH)₂ in the baseline voltammogram. This ratio was confirmed using a second Ni_{Black} electrode. Therefore, to calculate our nickel surface areas we calculated the charge for the formation of α -Ni(OH)₂ in the baseline voltammogram and multiplied this value by 2.57, before converting that value into μ mols of surface atoms. This method provides a surface area greater than would be obtained from the cyclic voltammogram method alone, the implications of which will be addressed in Chapter 3.

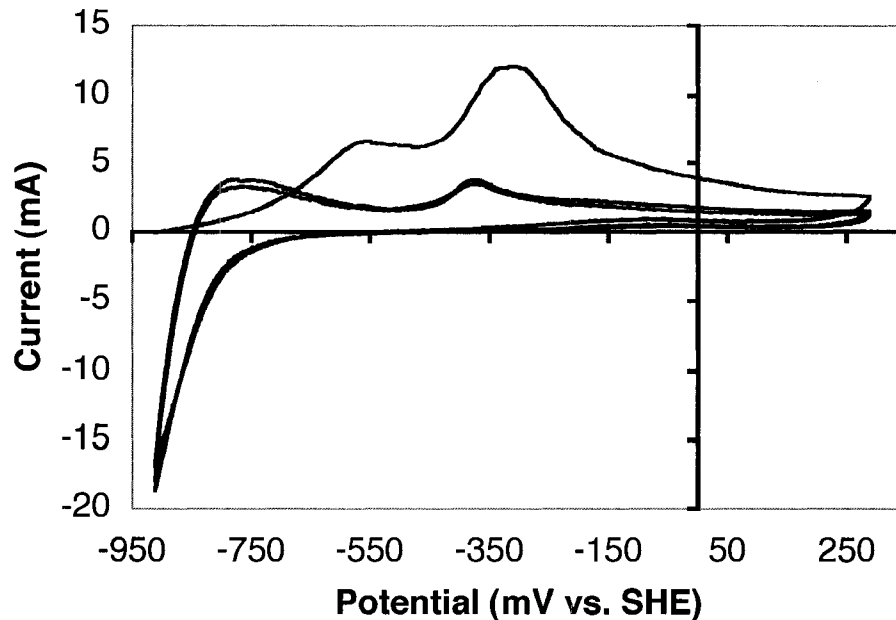


Figure 2-13: CO stripping voltammetry on a Ni/Pt electrode in 0.5 M NaOH sweeping at 10mV s^{-1} for 2 sweeps.

Figure 2-13 shows the CO stripping voltammogram of a Ni/Pt electrode in 0.5 M NaOH. Again, there exist two distinctive peaks, one at -550 mV and a second at -340 mV . Both peaks are in nearly the same location as the peaks for Ni_{Black} electrodes. This behavior was expected because of the high ratio of nickel to platinum deposited. Specifically, the atomic composition of the Ni/Pt electrodes was typically around 1.8% Pt.

It was unclear why the peak at -375 mV remained following the stripping of adsorbed CO. This peak, to the best of our knowledge, has not been reported previously. We believe that irreversible surface oxidation

occurred at the high potentials required for the stripping, possibly forming a platinum oxide.

The real electrochemical area of the Ni/Pt electrode was calculated in a manner similar to that of the Ni_{Black} electrodes. The CO stripping area for this electrode the area corresponded to a total charge of 0.4107 C.

We correlated this value to a consistent region of the Ni/Pt cyclic voltammogram. Unlike the platinum voltammogram, there were no reductive hydride peaks, and so we were unable to calculate the surface area in the same way as for Pt_{Black} electrodes. Similarly, there was no nickel oxidation peak in the Ni/Pt cyclic voltammogram so the technique for Ni_{Black} electrodes could not be used either. As a result we decided to take the total anodic charge from the cyclic voltammogram of the Ni/Pt electrode, from -835 mV to -650 mV in Figure 2-10. From our data we observed that the CO stripping charge was 1.58 times greater than the charge obtained from the cyclic voltammogram. Therefore, to calculate our Ni/Pt electrode surface areas we calculated the total anodic charge from the cyclic voltammogram and multiplied it by the factor of 1.58 before converting that value into μmols of surface atoms. These were the values used as normalization factors for the comparison of currents, as will be discussed further in Chapter 3.

CO adsorption and stripping on platinum has been extensively studied, the CO stripping peak on platinum occurs at a potential of 0.019 V vs. SHE in 0.1 M NaOH.⁸³ Our hope was to identify a peak corresponding to the oxidation

of CO from platinum in this voltammogram. While a distinctive peak was not observed, we did observe some unusual behaviors in the potential region from -200 mV to ~ 0 mV. Specifically, the decay of the second peak of the first sweep of the Ni-CO stripping voltammogram did not proceed smoothly, but appeared to be combined with a second process of lesser magnitude. We believe that the behavior in this region is due to CO oxidation from platinum. Unfortunately, the peak is too small and undefined to properly calculate its charge. This would appear to suggest that very little platinum is located on the surface of the electrode. However, 1.8 μmols of platinum were deposited and the real surface area of the electrode was determined to be 3.34 μmols of surface atoms. These values indicate that, if all the platinum were located on the surface of the electrode, the surface composition would be approximately 50% platinum. On the other hand, it is also possible that no platinum is located on the surface, though this extremely unlikely considering our previous observations. As a result, we know for certain that the surface of our electrodes is between 0% and 50% platinum, though neither extreme is expected. We do however, believe that more platinum is located on the surface than not, because the cyclic voltammogram had nearly no nickel character and because of the activity of the Ni/Pt electrodes towards H_2O_2 . These results are contradictory and suggest that further investigation is necessary.

Chapter 3: Electrochemical Activity of Ni/Pt Electrodes Towards the Electrooxidation of 2-Propanol in Base

3.1 Potentiodynamic Electrooxidation of 2-Propanol: Three electrode experiments were performed to determine the activity of the Ni/Pt electrodes towards the electrooxidation of 2-propanol in base. Figure 3-1 shows the cyclic voltammogram of a Pt_{Black} electrode in 0.5 M NaOH and in 1 M 2-propanol/ 0.5 M NaOH at 60°C. Bergens group member Matthew Markiewicz has studied the oxidation of 2-propanol over blacked platinum gauzes in alkaline electrolytes in great detail.⁴⁶ The potentiodynamic response of Pt_{Black} in NaOH is typical.⁸⁴

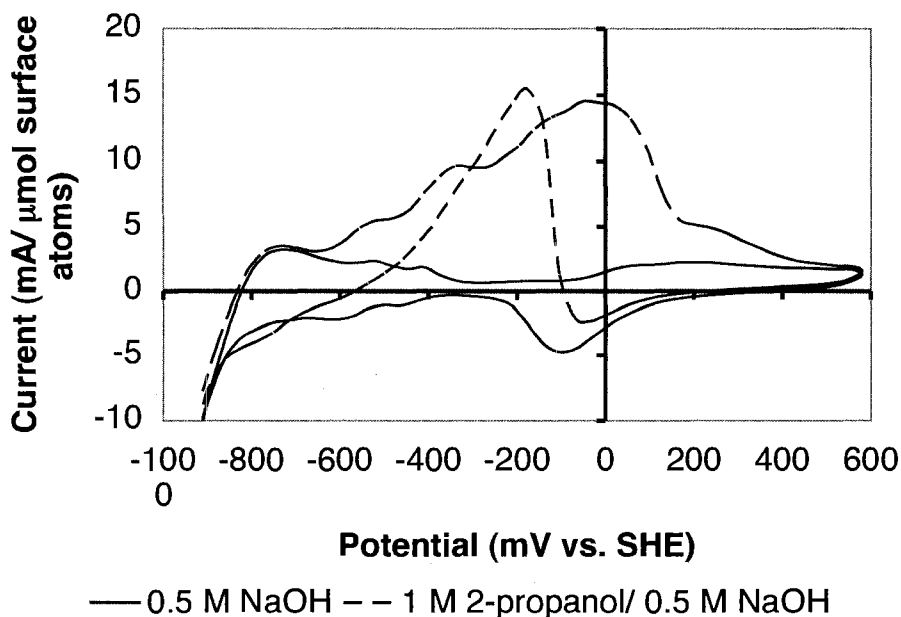


Figure 3-1: Potentiodynamic electrooxidation of 1 M 2-propanol in 0.5 M NaOH at 60°C over a Pt_{Black} electrode at a scan rate of 10 mV s⁻¹.

The standard potential for the oxidation of 2-propanol to acetone is –697 mV. Here, the onset of 2-propanol oxidation is at –650 mV and peaks at 0 mV. During the electrooxidation, the voltammogram retains elements of structure consistent with the hydride region of platinum in alkaline electrolytes, specifically, the three peaks at potentials less than –400 mV. Two products are formed by the electrooxidation of 2-propanol in basic electrolytes.⁴⁶ At low potentials the oxidation occurs in the absence of strongly adsorbed species and forms acetone as the major product. At high potentials a second mechanism predominates, and the current is limited by the formation of strongly adsorbed species and the formation of surface oxides. The adsorbed species are due to the oxidation of acetone to carbon dioxide at high potentials. The surface oxides are reduced at ~ 50 mV in the reverse sweep and results in a dramatic increase in current.

In comparison, Figure 3-2 shows the baseline cyclic voltammogram of Ni_{Black} in 0.5 M NaOH, and stabilized potentiodynamic response for the electrooxidation 2-propanol over Ni_{Black}.

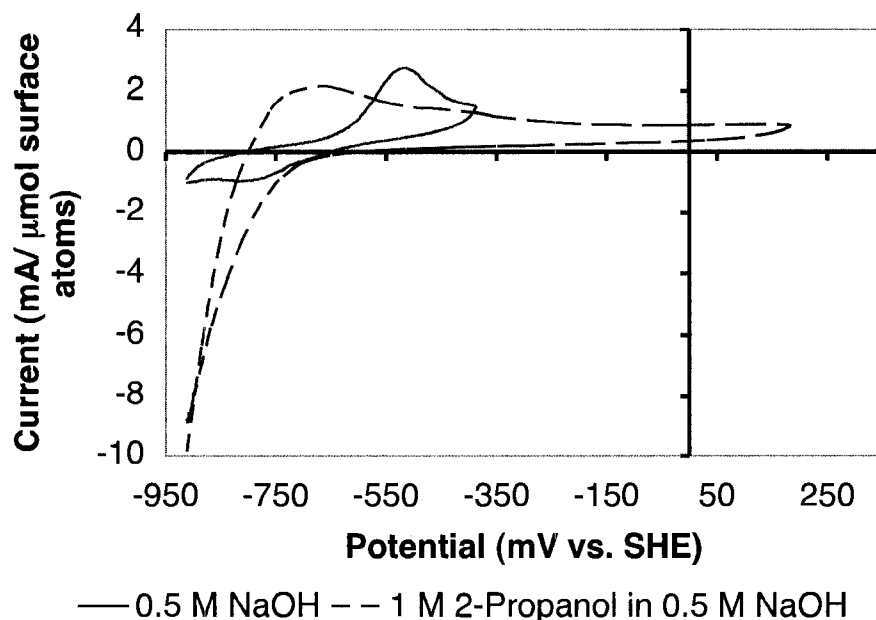


Figure 3-2: Potentiodynamic electrooxidation of 1 M 2-propanol in 0.5 M NaOH at 60°C over a Ni_{Black} electrode at a scan rate of 10 mV s⁻¹.

The baseline cyclic voltammogram (-912 mV to -380 mV) was recorded immediately following the Ni_{Black} deposition, and the potentiodynamic voltammogram (-912 mV to 180 mV) was taken subsequent to other analyses. In the time between these two experiments the electrode surface aged, as indicated by the loss of peaks characteristic of the Ni(OH)₂ redox couple from the cyclic voltammogram. Aging of nickel electrodes is a well-studied phenomenon that is known to occur at high potentials, upon standing in alkaline media and upon standing in air.^{85,86,87,88,89,90} We endeavored to minimize this aging by limiting the upper potential limit of the cyclic voltammograms to less than -380 mV, and by limiting the time the electrode was left sitting in the electrolyte. Sweeping to high potentials was required

because no 2-propanol oxidation was observed at potentials less than -380 mV.

The potentiodynamic response in Figure 3-2 shows that, unlike platinum, the Ni_{Black} electrode does not oxidize 2-propanol. Specifically, no increase in current is observed at high potentials in the presence of 2-propanol. Sweeping the Ni_{Black} electrodes to these high potentials resulted in heavily oxidized surfaces, rendering the electrodes useless for further investigations. Alone, nickel is therefore not an effective electrocatalyst for the electrooxidation of 2-propanol.

Figure 3-3 shows the original cyclic voltammogram (-912 mV to -380 mV) of a Ni/Pt electrode in 0.5 M NaOH and the first sweep for the potentiodynamic electrooxidation (-912 mV to 180 mV) of 2-propanol over the same electrode. The upper potential limit of the cyclic voltammogram was set to -380 mV, in order to limit the formation of nickel oxides and electrode aging, as previously discussed. We do not know what effect the platinum in the Ni/Pt electrodes has on electrode aging, so the same precautions were taken as with the Ni_{Black} .

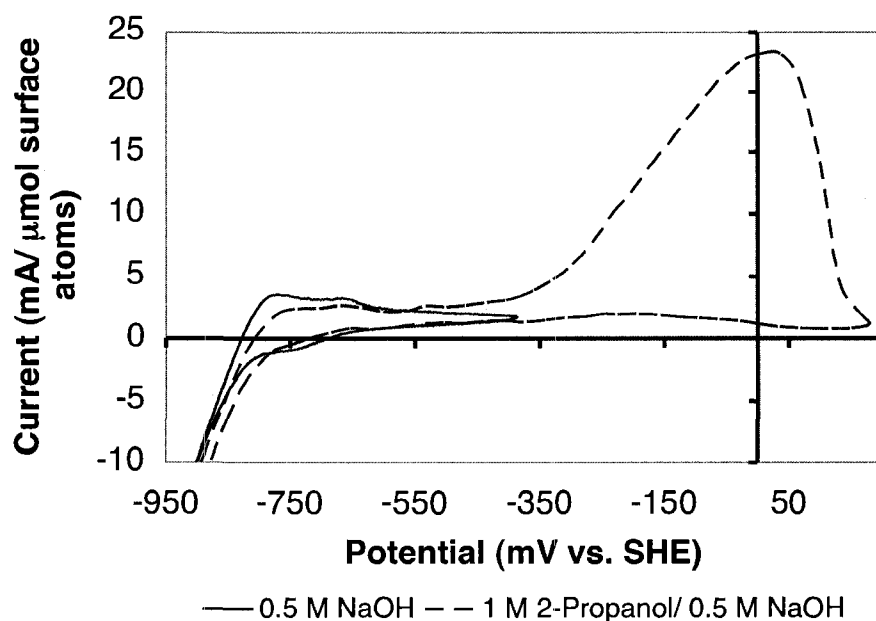


Figure 3-3: Potentiodynamic electrooxidation of 1 M 2-propanol in 0.5 M NaOH at 60°C over a Ni/Pt electrode at a scan rate of 10 mV s⁻¹.

No current was observed in the reverse sweep of the potentiodynamic electrooxidation of 2-propanol. The electrode was passivated at the very high anode potentials used in this experiment. We did not do the experiments in which we would have gradually increased the upper limit over successive sweeps to determine at which potential passivation occurs.

Figure 3-4 shows the normalized potentiodynamic responses of Pt_{Black}, Ni_{Black}, and Ni/Pt electrodes towards the electrooxidation of 2-propanol.

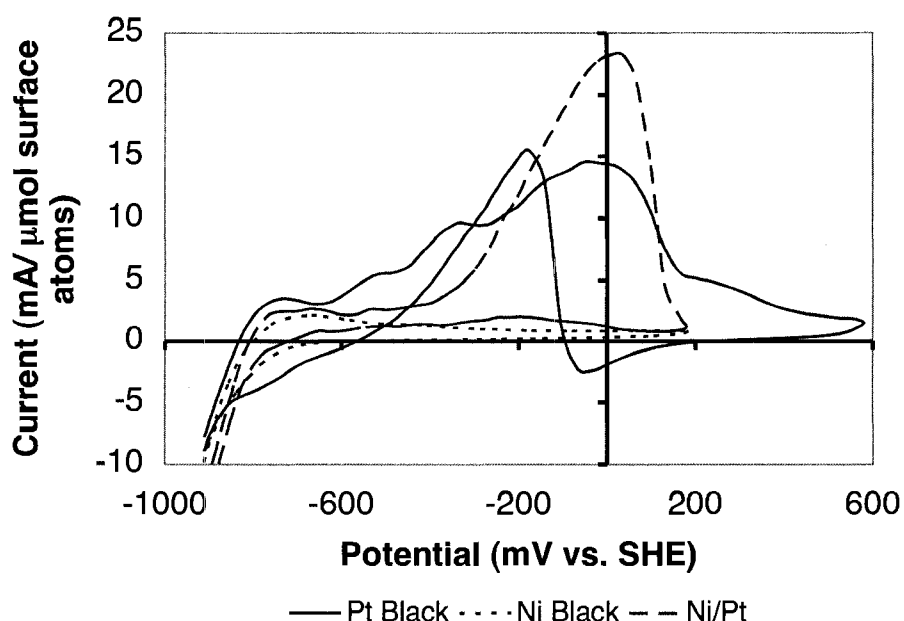


Figure 3-4: Potentiodynamic electrooxidation of 1 M 2-propanol in 0.5 M NaOH at 60°C over Pt_{Black}, Ni_{Black}, and Ni/Pt electrodes.

The onset potential for 2-propanol oxidation is approximately 250 mV lower over Pt_{Black} than over Ni/Pt, but the maximum current obtained for Ni/Pt in the first sweep was nearly 8 mA (μmol surface atoms)⁻¹ greater than for Pt_{Black}. As discussed above, Ni_{Black} electrodes are inactive in this potential region, and therefore any activity over Ni/Pt electrodes must inherently be due to the presence of platinum. This observation shows that the incorporation of a small amount of platinum within a nickel matrix promotes the electrooxidation of 2-propanol. The high activity of the Ni/Pt electrodes implies that most of the platinum is located near the surface, but the total amount of platinum on the surface of the Ni/Pt electrodes is much less than the total amount of platinum on the surface of the Pt_{Black} electrodes. To illustrate this, the relative amounts of surface platinum on Ni/Pt electrodes and Pt_{Black} electrodes respectively, can

be compared. During electrodeposition, 1.8 μmols of platinum were deposited into the Ni/Pt electrode and the surface area was 3.34 μmols of surface atoms but, as discussed in Chapter 2, it is unlikely that all of the platinum is located on the electrode surface. The surface area of the Pt_{Black} electrode, on the other hand, was 9.21 μmols of surface atoms, and the surface consisted entirely of platinum. Despite the significant difference in composition, bulk platinum was less active than the small amount of highly dispersed platinum in the Ni/Pt framework. Similar behavior is observed with Pt/Ru electrodes relative to Pt. The role of the ruthenium in these electrocatalysts is to provide oxides that help remove adsorbed species by promoting the formation of CO₂.⁵⁰ Nickel also forms oxides it is possible that at low potentials these nickel oxides also help to promote the removal of adsorbed species from platinum. As mentioned in Chapter 1, the presence of nickel can serve to decrease the binding energy of platinum in Ni-Pt electrodes, weakening the Pt-CO bond and therefore decreasing poisoning of the catalyst surface.^{62,63}

3.2 Potentiostatic Electrooxidation of 2-Propanol: Analysis of the potentiostatic current-time response for the oxidation of 2-propanol provides a more realistic assessment of the behavior of the 2-propanol/ Ni/Pt system in an operating fuel cell. Before each experiment the electrode was conditioned at -1212 mV vs. SHE for 5 minutes to reduce the surface of the electrode. The potential was then stepped to the desired potential and the current was

recorded over 15 minutes. The reported current is the average of the last 5 seconds of the 15-minute experiment. Figure 3-5 shows the potentiostatic response of 2-propanol over a Pt_{Black} electrode. The currents reported here are not normalized to the surface area of the Pt_{Black} electrode. This was done to provide a sense of the absolute currents that were obtained from these electrodes.

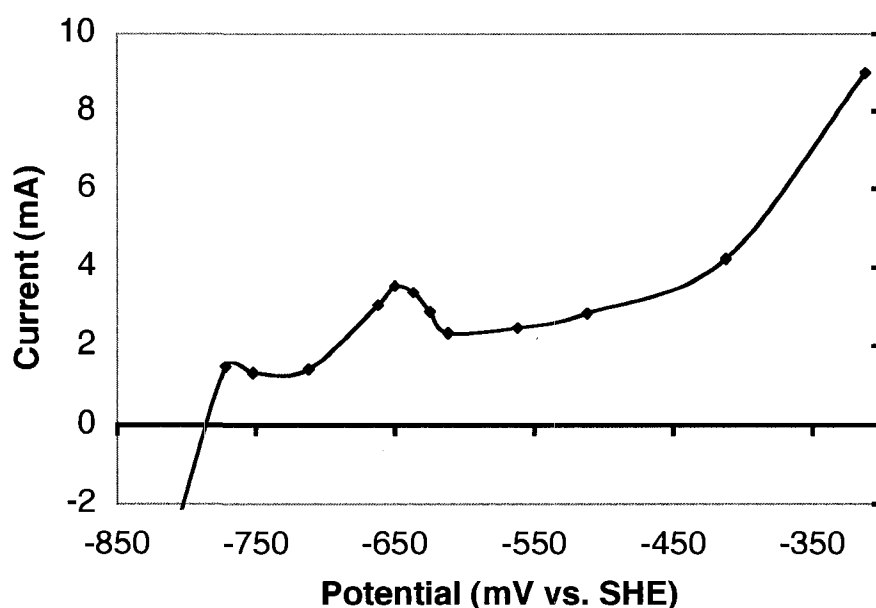


Figure 3-5: Unnormalized potentiostatic currents at 15 minutes for the electrooxidation of 1 M 2-propanol in 0.5 M NaOH at 60°C over Pt_{Black}.

Our group has studied the electrooxidation of 2-propanol over blacked platinum gauzes extensively, Figure 3-5 is typical.⁴⁶ A significant current maximum occurs at low potentials (~ -650 mV) due to the rapid partial oxidation of 2-propanol to acetone. Figure 3-5 shows the onset of 2-propanol oxidation is at -712 mV. This potential is lower than the potentiodynamic

onset potential discussed in Section 3.1, but closer to the standard reduction potential of -697 mV for this reaction. Following the onset of oxidation there occurs a period of decreased current in the region from -650 mV to -600 mV where the onset of acetone oxidation begins to inhibit 2-propanol oxidation. Following this, a second region of current increase occurs from -600 mV to -300 mV, where the oxidation of 2-propanol is, again, the primary reaction.

Figure 3-6 shows the same potentiostatic current for the electrooxidation of 2-propanol normalized to the real electrochemical surface area of the Pt_{Black} electrode.

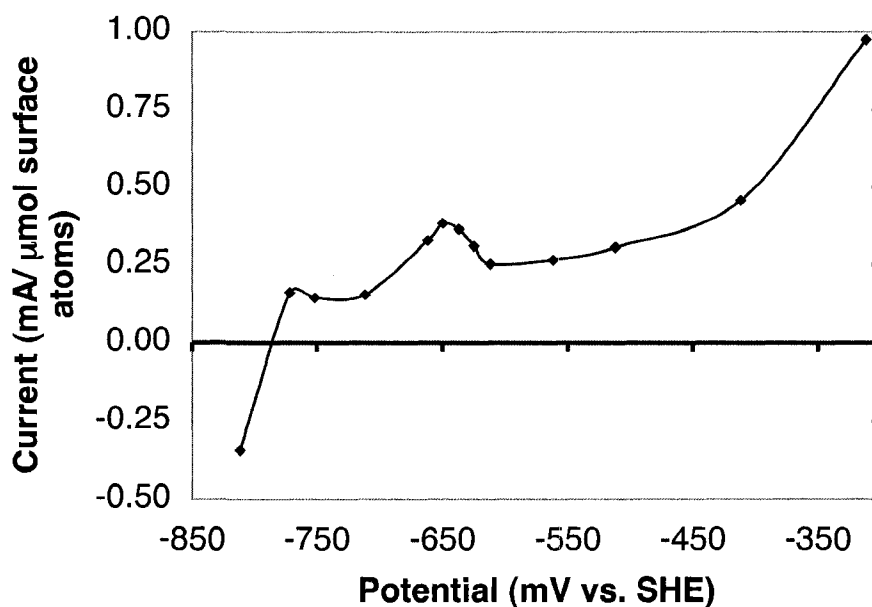


Figure 3-6: Normalized potentiostatic current for the electrooxidation of 1 M 2-propanol in 0.5 M NaOH at 60°C over a Pt_{Black} electrode.

Figure 3-7 shows the unnormalized potentiostatic currents for the electrooxidation of 2-propanol over Ni_{Black} .

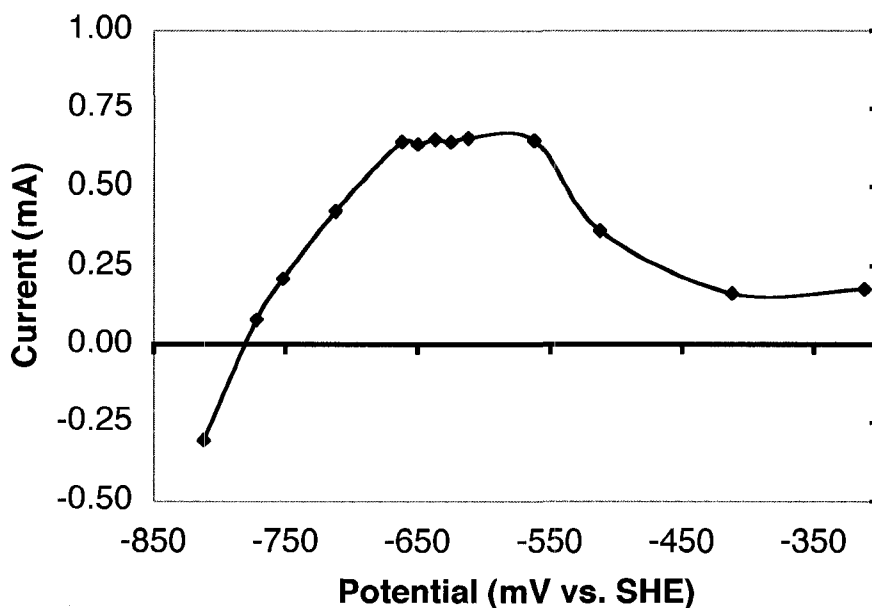


Figure 3-7: Unnormalized potentiostatic currents at 15 minutes for the electrooxidation of 1 M 2-propanol in 0.5 M NaOH over a Ni_{Black} electrode.

We were surprised to find that nickel was, apparently, capable of electrooxidizing 2-propanol at low potentials in alkaline media. This behavior is contrary to the response observed during the potentiodynamic electrooxidations. Specifically, the potentiodynamic electrooxidations showed no increased current over the potential range studied, indicating that Ni_{Black} was not an effective catalyst for the oxidation of 2-propanol. We therefore suspected that the currents observed in Figure 3-7 were due to oxidation of the electrode surface rather than oxidation of 2-propanol.

To test this hypothesis, the same potentiostatic electrooxidation experiments were performed on a fresh Ni_{Black} electrode in the absence of 2-propanol. The results of these experiments revealed that oxidation of the electrode does indeed occur under these conditions. Figure 3-8 shows the

normalized current obtained under potentiostatic conditions in the absence of 2-propanol.

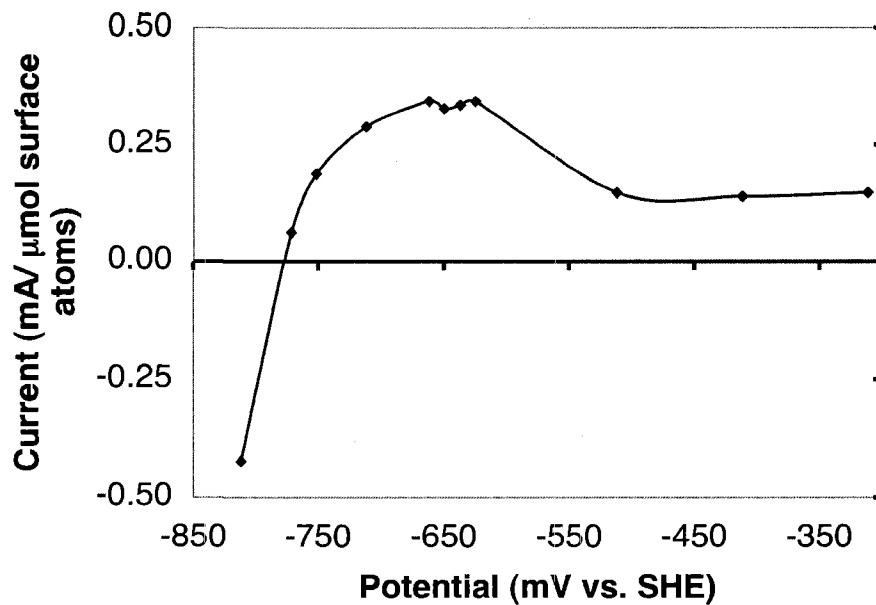


Figure 3-8: Potentiostatic electrooxidation of a Ni_{Black} electrode in 0.5 M NaOH at 60°C

Figure 3-9 shows the result of subtracting the potentiostatic current obtained in the absence of 2-propanol from the potentiostatic current obtained in its presence.

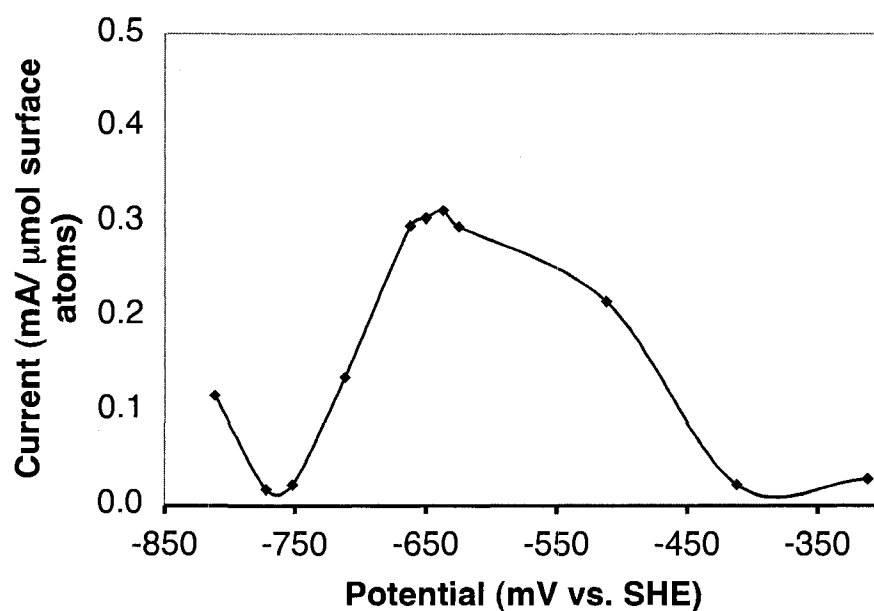


Figure 3-9: Subtraction of the potentiostatic current obtained in the absence of 2-propanol from the potentiostatic current obtained in the presence of 2-propanol, normalized to the CO stripping surface area of the Ni_{Black} electrode.

The positive currents after subtraction may indicate that Ni has some activity towards 2-propanol under these conditions. This data is difficult to interpret however, because 2-propanol may have an effect on the oxidation kinetics of Ni in base. This matter was not pursued further.

Figure 3-10 shows the unnormalized potentiostatic currents at 15 minutes for the electrooxidation of 1 M 2-propanol in 0.5 M NaOH over a Ni/Pt electrode.

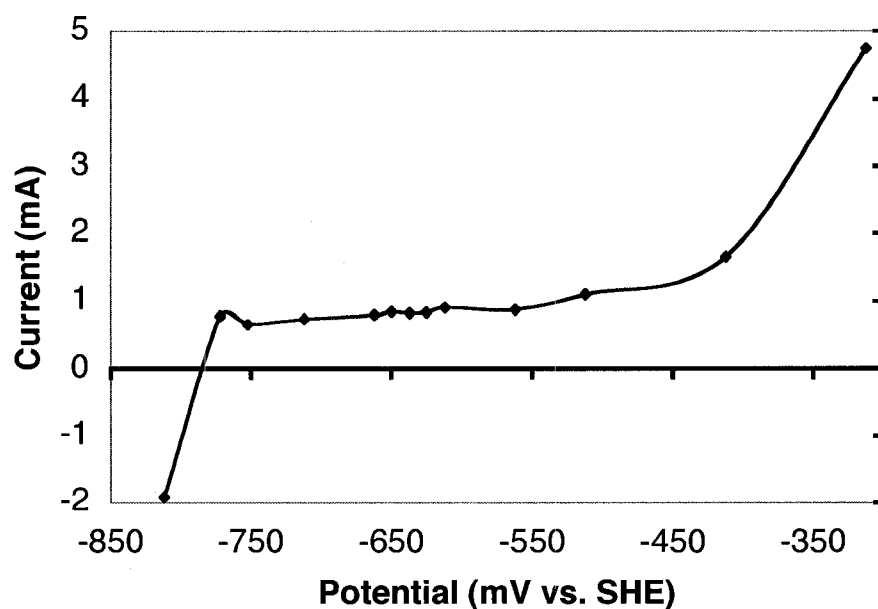


Figure 3-10: Unnormalized data for the potentiostatic electrooxidation of 1 M 2-propanol in 0.5 M NaOH over a Ni/Pt electrode.

The onset of alcohol oxidation begins near -790 mV and, following this onset, the stabilized currents increase linearly with increasing potential until -400 mV where there occurs a dramatic increase in the potentiostatic current. Figure 3-11 shows the stabilized potentiostatic current for the electrooxidation of 1 M 2-propanol, normalized to the real surface area of the Ni/Pt electrode, as discussed in Section 2.4.

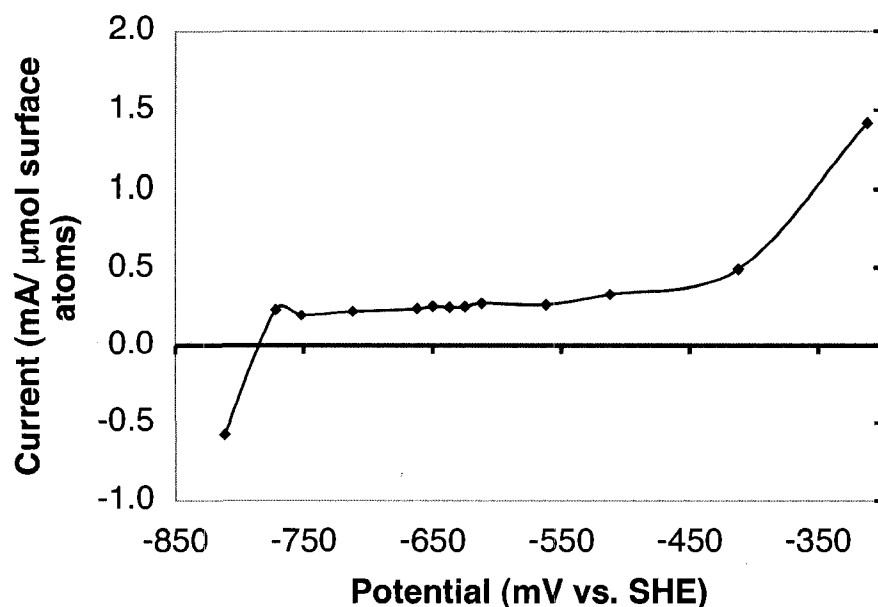


Figure 3-11: Normalized data for the potentiostatic electrooxidation of 1 M 2-propanol in 0.5 M NaOH over a Ni/Pt electrode.

The normalized currents have a magnitude near 0.25 mA ($\mu\text{mol surface atoms})^{-1}$ from -750 mV to about -500 mV. It should be noted that the current maximum near -650 mV, observed for the electrooxidation of 2-propanol over Pt_{Black} electrodes, was only observed once among the series of Ni/Pt electrodes prepared for this investigation so, in general, this does not seem to be a feature associated with Ni/Pt electrodes.

Figure 3-12 shows the potentiostatic currents for the oxidation of 2-propanol over Pt_{Black} , Ni_{Black} , and Ni/Pt electrodes. These currents have not been normalized to the real surface areas of the respective electrodes. In this way it is possible to see how the absolute activity of the Ni_{Black} and Ni/Pt electrodes is dependant on the nature of the electrode material.

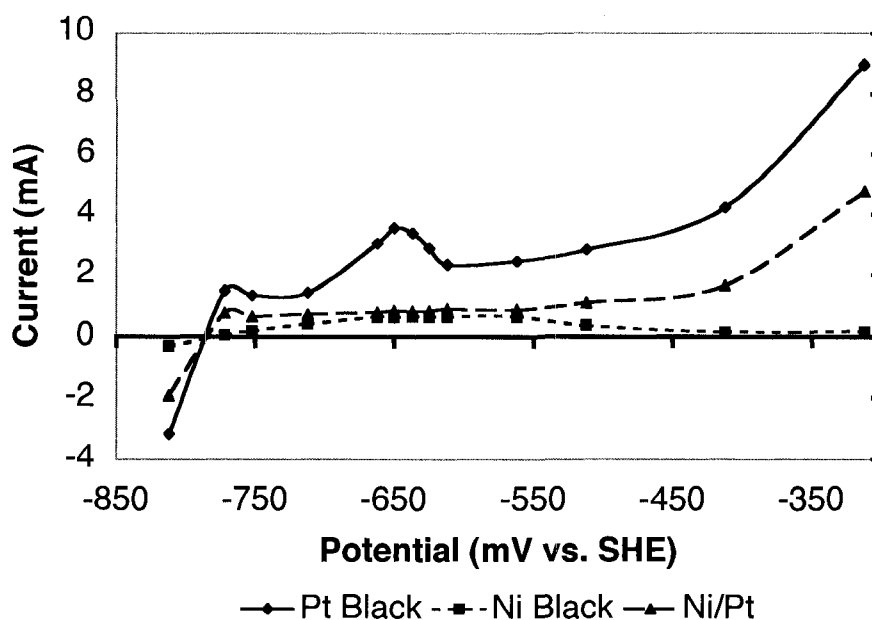


Figure 3-12: Comparison of the unnormalized potentiostatic electrooxidation currents over Pt_{Black}, Ni_{Black}, and Ni/Pt electrodes.

Here, we see that the absolute currents increase as the amount of platinum in the electrode increases. The real surface area of the Ni/Pt electrode was 3.34 μmol surface atoms and the Ni_{Black} electrode was 1.00 μmol surface atoms. This relative increase in real surface area with the amount of Pt was common to all the Ni/Pt electrodes prepared for this study. Therefore, the incorporation of platinum increases the surface area of the electrodes and these higher surface electrodes are able to sustain larger currents. The stability of these currents across this potential range indicates that the incorporation of platinum not only leads to the formation of high area surfaces, but that these surfaces are also stable in the potential region studied. In comparison, the real surface area of a typical blacked platinum gauze was 9.21 μmol surface atoms. Although the blacked platinum gauze was prepared under different conditions,

the higher surface area of the Pt gauze may be consistent with the apparent trends that the incorporation of Pt results in a higher surface area. As discussed previously, the Ni_{Black} electrode does produce oxidative currents at low potentials under these conditions that are at least in part due to oxidation of the nickel surface. It appears that the presence of Pt stabilizes the surface at low potentials in the presence of 2-propanol. This hypothesis must be studied using prototype 2-propanol fuel cells using Ni/Pt anode electrocatalysts.

A behavior common to all three electrodes is that the onset of 2-propanol electrooxidation occurs at -790 mV. Additionally, both the Pt_{Black} and Ni/Pt electrodes show a small increase in current directly following the onset of oxidation. This behavior is not due to hydrogen, as, over the 15 minutes, all hydrogen would have been removed from the system. Another similarity between Pt_{Black} and Ni/Pt is the steady increase in stabilized current that occurs between -600 mV and -400 mV and the dramatic increase in stabilized current that occurs at potentials more positive than -400 mV. Seeing how the Ni_{Black} does not display either of these behaviors, the activity of the Ni/Pt electrode undoubtedly is due to the small amount of platinum present.

Figure 3-13 shows the potentiostatic currents for the oxidation of 1 M 2-propanol normalized to the real surface areas of the respective electrodes. The Ni_{Black} data has been included for the purpose of discussion.

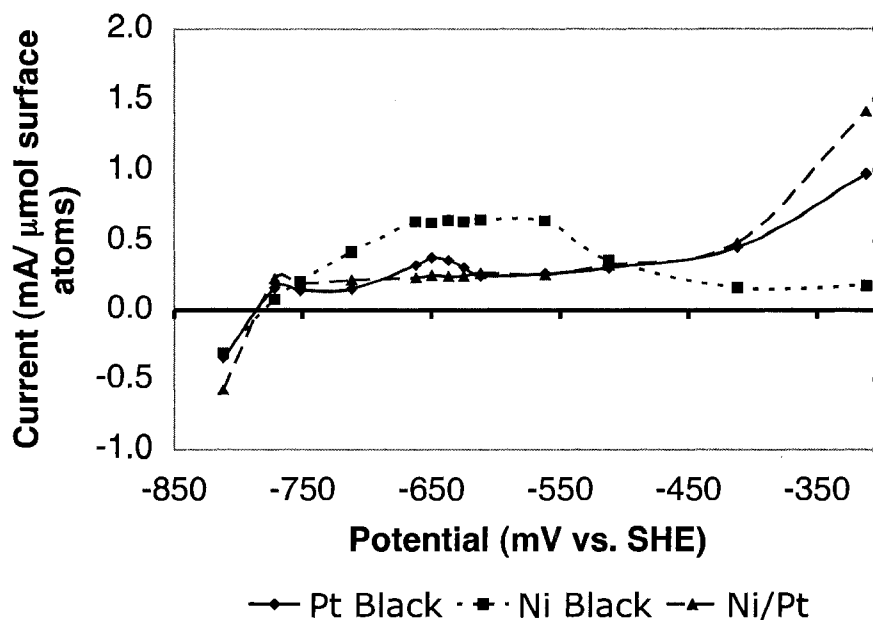


Figure 3-13: Comparison of the normalized potentiostatic electrooxidation currents over Pt_{Black} , Ni_{Black} , and Ni/Pt electrodes.

It was surprising that the normalized currents obtained over Ni/Pt were nearly equal to the normalized currents obtained over Pt_{Black} . Specifically, with the exception of the current maximum over Pt_{Black} at -650 mV, the currents were essentially identical in the potential range from approximately -800 mV to -450 mV. At potentials greater than -450 mV, the current increase over the Ni/Pt electrode was larger than the current increase over Pt_{Black} . This indicates that, in this potential region, the Ni/Pt electrodes are more active than Pt_{Black} towards the oxidation of 2-propanol despite having a much lower surface loading of platinum (maximum of $1.8 \mu\text{mols}$ for Ni/Pt versus $9.21 \mu\text{mols}$ for Pt_{Black}). This finding is in agreement with the behavior observed during the potentiodynamic electrooxidations. The normalized potentiostatic currents

over Ni were higher than Pt or Ni/Pt at low potentials. As shown previously, nickel is inactive towards 2-propanol in potentiodynamic oxidation experiments, and nickel undergoes oxidation in the absence of Pt and 2-propanol at low potentials in potentiostatic experiments. We suspect that the majority of the currents over Ni_{Black} at low potentials are due to oxidation of nickel. We note that the presence of Pt appears to stabilize the surface towards this oxidation, and favors oxidation in 2-propanol instead. This hypothesis will be tested using prototype fuel cells.

As a result of these experiments we were able to make several conclusions. First, the presence of platinum in the Ni/Pt electrode promotes the formation of a higher surface area electrode. This higher surface electrode is capable of sustaining larger unnormalized currents than Ni_{Black} electrodes. Second, at high potentials the Ni/Pt electrodes produce a greater normalized current maximum than Pt_{Black} electrodes. Third, normalized potentiostatic currents over Ni/Pt and Pt_{Black} electrodes are nearly identical at low potentials. At high potentials, Ni/Pt is more active towards 2-propanol oxidation than Pt_{Black}. Fourth, the oxidation of Ni_{Black} under these conditions makes it impossible to properly compare its activity to that of Ni/Pt and Pt_{Black}, though, from the potentiodynamic response in 2-propanol, we are confident that Ni_{Black} is essentially inactive towards 2-propanol oxidation.

3.3 Conclusion and Application to an Operational Fuel Cell: Our data indicates that Ni/Pt electrodes are probably best suited for operation at potentials less than -380 mV. In both the potentiodynamic and potentiostatic experiments, Ni/Pt electrodes had activity comparable to, or better than Pt_{Black} electrodes towards the oxidation of 2-propanol, despite having lower Pt surface loadings. This indicates that Ni/Pt electrodes are, in principle, suited for operation in fuel cells at low potentials. This is in harmony with the conditions for optimal fuel cell operation whereby the anode is held at a low potential in order to obtain the largest possible potential difference between the electrodes. Further research is necessary to assess the suitability of these electrodes to operational fuel cell conditions.

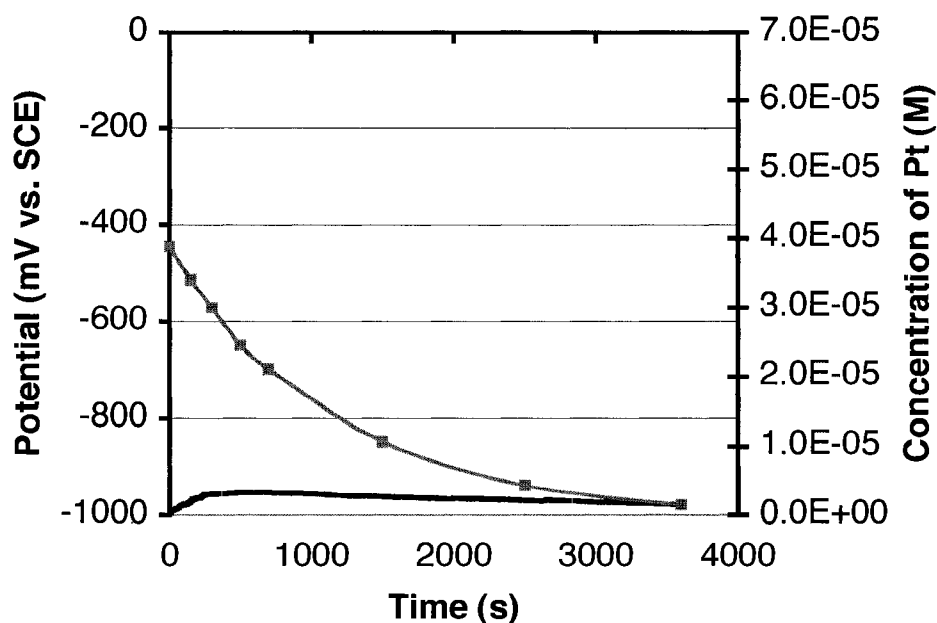
Chapter 4: Conventional Co-Deposition of Ni+Pt Electrodes Using Platinum Metal Salt Precursors

4.1 Galvanostatic Co-Deposition of Ni+Pt electrodes: Our method for preparing Ni/Pt anodes is previously unreported. The usual means by which such materials are obtained is through controlled co-deposition from solutions of the respective metal salts. Our Ni/Pt electrodes have very low platinum loadings and, to our understanding, have not been produced by conventional means. As our anode has proven to be active towards the electrooxidation of 2-propanol in alkaline electrolytes, we wished to attempt to prepare Ni/Pt electrodes via the conventional method using both zeise's salt and chloroplatinic acid as platinum sources. The reason for using these precursors was two-fold: first we wished see if it was possible to obtain an active catalyst of approximately the same composition using conventional deposition and second, we wished to know if the oxidation state of platinum had an effect on the deposition process.

Four controlled galvanostatic co-depositions were performed using the same electrochemical parameters as for the galvanostatic deposition of our Ni/Pt electrodes. Either H_2PtCl_6 or $\text{K}[\text{PtCl}_3(\text{C}_2\text{H}_4)] \cdot \text{H}_2\text{O}$ was added to a 0.2 M NiCl_2 / 2.0 M NH_4Cl solution. Both of these platinum precursors were selected because they contain chlorides, this minimized interference from ligand species not originally present in the original deposition solution. The exception

to this was the ethylene ligand from $K[PtCl_3(C_2H_4)] \cdot H_2O$. These electrodes will be referred to from now on as the conventionally co-deposited Ni+Pt electrodes.

Figure 4-1 shows the deposition behavior of two electrodes with different starting concentrations of chloroplatinic acid. These starting concentrations were selected to be slightly less and slightly more than the concentration maximum of platinum observed during the deposition of Ni/Pt electrodes in section 2.1. Aliquots of the deposition solution were taken at specific times to monitor the concentration of platinum during the deposition.



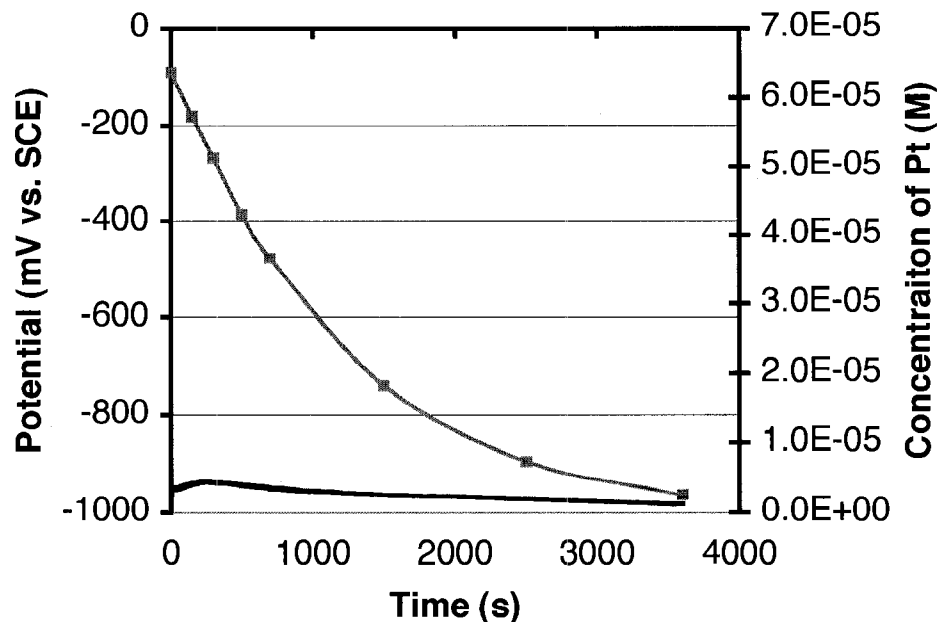


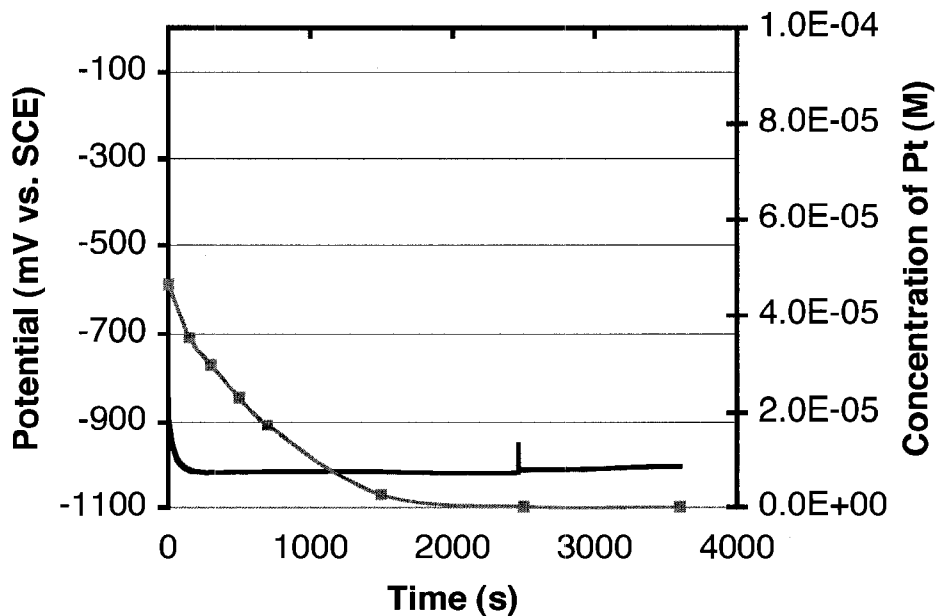
Figure 4-1: Deposition potential of the electrode and the concentration of H_2PtCl_6 in solution during galvanostatic electrodeposition at -0.1 A .

The concentration of platinum in these deposition solutions decreases in the same quasi-exponential way that was observed during our original Ni/Pt electrode deposition. After one hour, the remaining concentration of platinum in solution is essentially zero.

Unlike the case of our Ni/Pt electrodes, a dramatic increase in potential after the first 500 seconds does not occur and we did not observe potential stabilization near -400 mV as was observed in the Ni/Pt preparations. The absence of potential stabilization near -400 mV is surprising because the reduction of H^+ to form hydrogen over platinum occurs at less negative potentials than the reduction of nickel or platinum, as discussed previously.

Instead, after a short period of polarization, the deposition potentials for both electrodes remain nearly constant near -975 mV. Minimal gas evolution was observed during the conventional co-depositions. In fact, the absence of gas evolution and the low stable deposition potential were reminiscent of the deposition behavior of Ni_{Black} electrodes.

We believed that it was possible that platinum in the 4+ oxidation state was responsible for the unexpected potential behavior observed and so we performed the same controlled co-depositions using Zeise's Salt, a Pt^{2+} precursor. Figure 4-2 shows the deposition behaviors of two electrodes with different starting concentrations of Pt^{2+} . It should be noted that the electrode used for the first of the two depositions was slightly larger than the second and that the deposition was started, stopped immediately and restarted.



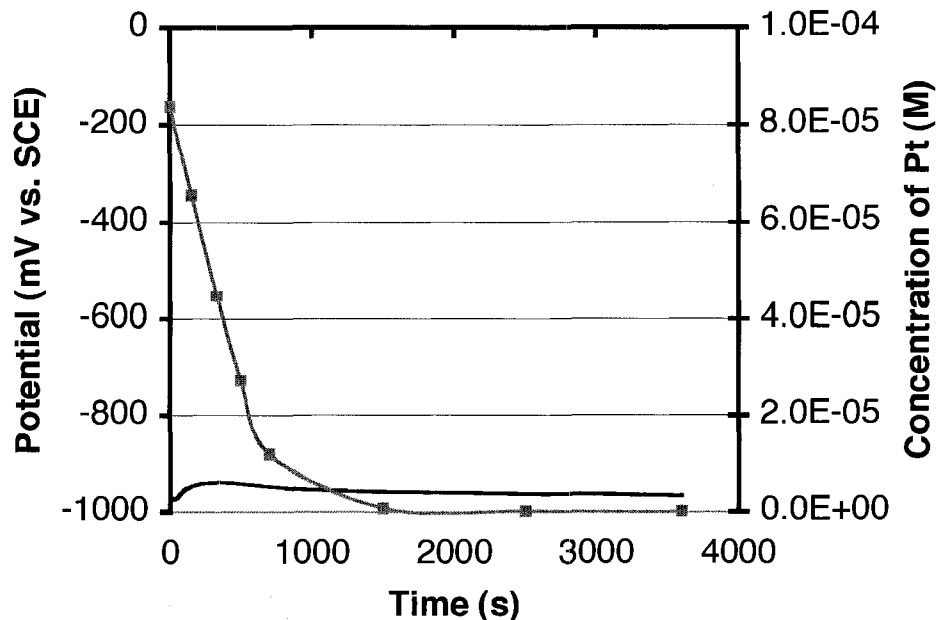


Figure 4-2: Deposition potential of the electrode and concentration of $\text{K}[\text{PtCl}_3(\text{C}_2\text{H}_4)] \cdot \text{H}_2\text{O}$ in solution over time during galvanostatic electrodeposition at -0.1 A .

The deposition potential for both of these electrodes again remained stable at low potentials and no significant hydrogen evolution was observed. From these observations it is clear that the oxidation state of the platinum precursor does not instigate the Ni_{Black} -like deposition behavior.

The oxidation state of the platinum precursor did however appear to have an effect how quickly platinum was deposited. Observation of the concentration of platinum in the deposition bath as a function of time shows no quasi-exponential decay, but rather a more dramatic decrease in

concentration that occurs over a shorter period of time. Specifically, the concentration of platinum in solution is nearly zero after only 1500 seconds.

As a result of these observations, two conclusions can be made as to the effect of oxidation state on the deposition of these Ni+Pt electrodes: first, the deposition of Pt^{2+} is more facile than the deposition of Pt^{4+} and second, it is plausible that the platinum originating from the counter electrode during the Ni/Pt electrode depositions is in the 4+ oxidation state. Unfortunately, neither of these conclusions explained the lack of activity of the co-deposited platinum towards the reduction of hydrogen in solution.

As before, the mass of each of the electrodes was obtained before and after deposition to monitor the absolute weight gain of each electrode. Figure 4-3 shows the average mass increases of the three types of electrodes following deposition.

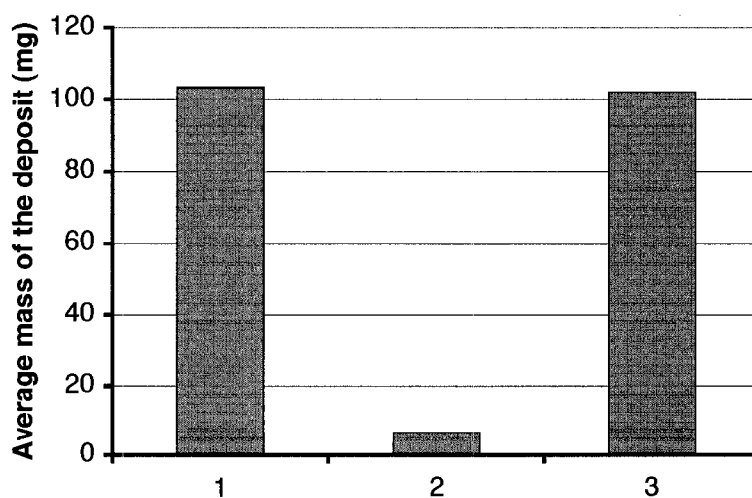


Figure 4-3: Average mass deposited onto (1) Ni_{Black} electrodes (2) Ni/Pt electrodes and (3) conventionally co-deposited Ni+Pt electrodes.

We were surprised to find another behavior similar to that of the Ni_{Black} electrodes. Not only were the deposition potential behaviors similar, the average masses gained by the four conventionally co-deposited Ni+Pt electrodes were nearly identical to the average mass gain of the Ni_{Black} electrodes. As discussed in Chapter 2, the smaller mass gain by the Ni/Pt electrodes is due to the diversion of current towards the production of hydrogen rather than the deposition of metal. The conventionally co-deposited Ni+Pt electrodes did not produce hydrogen during the deposition. As a result, the current was directed towards the reduction of platinum and nickel in solution. This would result in a greater net mass increase.

The co-deposited Ni+Pt electrodes were dissolved in aqua regia and their platinum content analyzed with ICP after all other experiments had been performed. The results of the ICP analysis are illustrated in Figure 4-4.

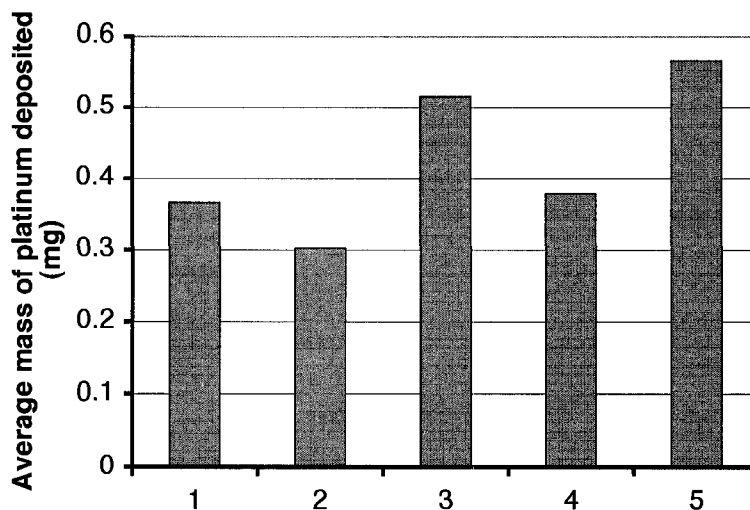


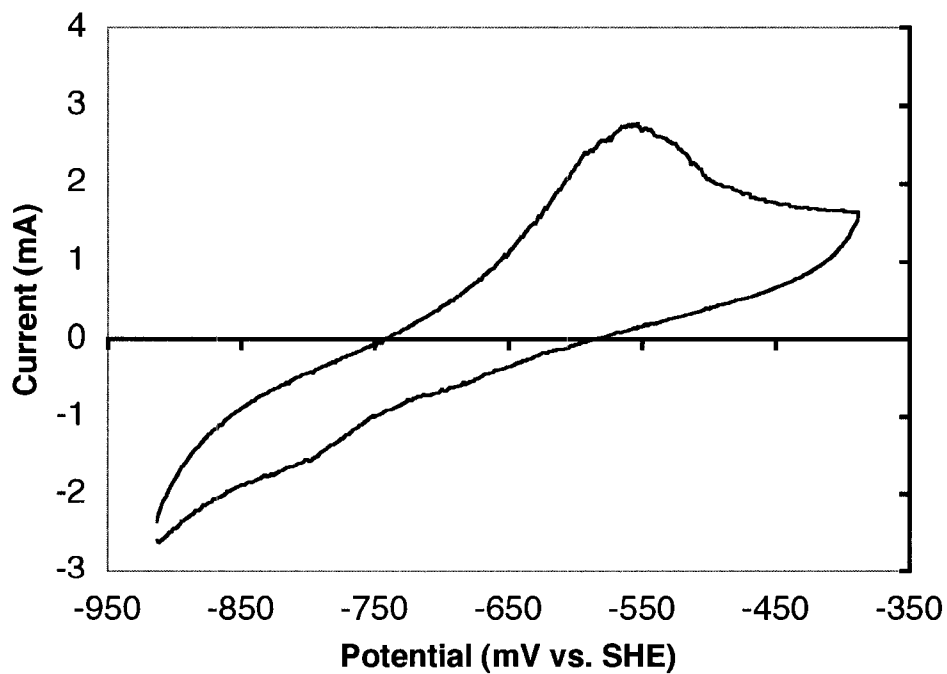
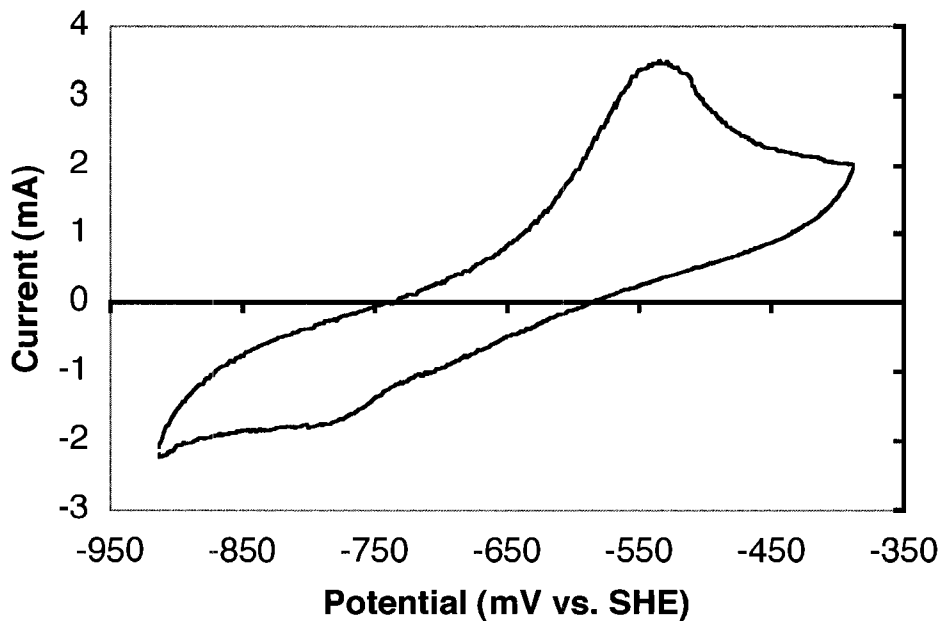
Figure 4-4: Mass of Pt deposited onto the (1) Ni/Pt electrodes (average), (2) 133 μL of 0.01483 M H_2PtCl_6 electrode, (3) 250 μL of 0.01483 M H_2PtCl_6 electrode, (4) 133 μL of 0.01520 M $\text{K}[\text{PtCl}_3(\text{C}_2\text{H}_4)]\cdot\text{H}_2\text{O}$ electrode and (5) 250 μL of 0.01520 M $\text{K}[\text{PtCl}_3(\text{C}_2\text{H}_4)]\cdot\text{H}_2\text{O}$ electrode.

From the ICP results it is clear that the platinum in solution was indeed deposited onto the electrodes. It is also clear that these four co-deposited Ni+Pt electrodes contained an equivalent or greater amount of platinum than the average Ni/Pt electrode.

The simple, qualitative yes/no H_2O_2 experiment resulted in no oxygen evolution over any of the four electrodes. This test confirmed that platinum was not present on the surface of the electrodes. The reason why platinum was not present on the surface is still unknown.

4.2 Voltammetry of the Co-Deposited Electrodes: Cyclic voltammograms of the co-deposited Ni+Pt electrodes were taken in 0.5 M NaOH. Figure 4-5

shows the cyclic voltammograms after deposition for the four conventionally co-deposited Ni+Pt electrodes.



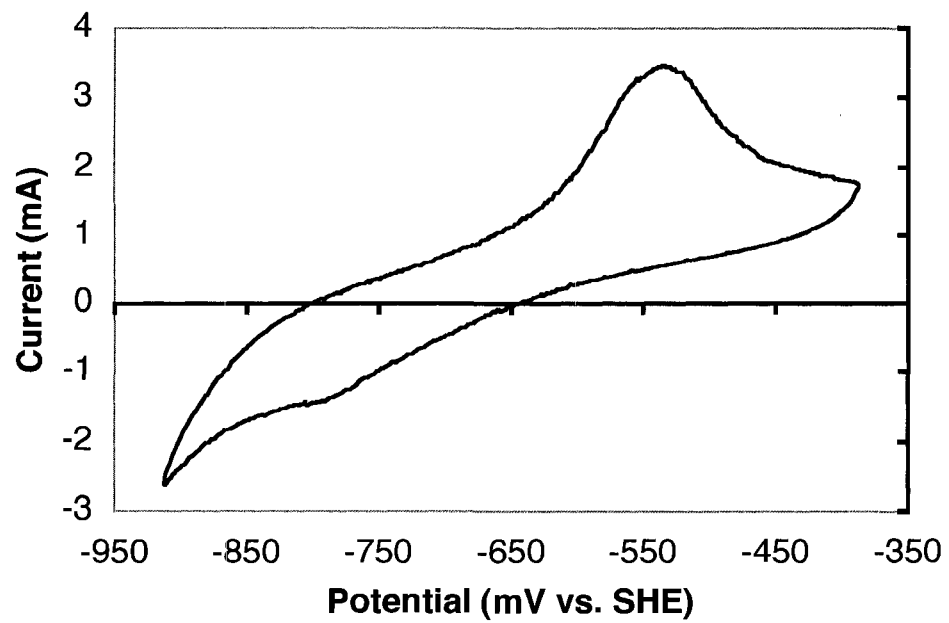
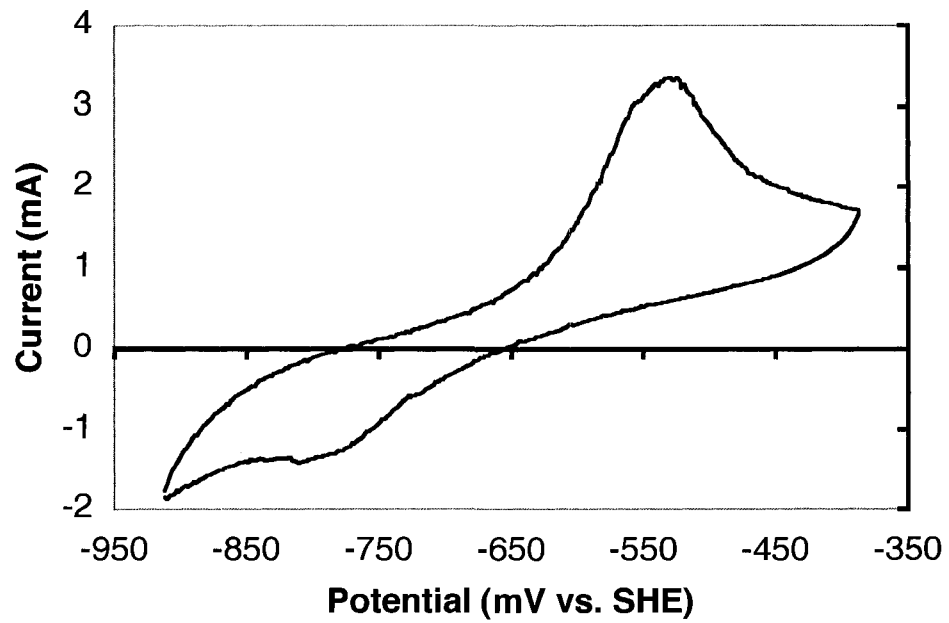


Figure 4-5: Cyclic voltammograms of the four conventionally co-deposited electrodes.

The cyclic voltammograms are all characteristic of the behavior of Ni_{Black} in alkaline electrolytes. Specifically, a distinctive peak is observed at -550 mV which is known to correspond to the oxidation of nickel to form α -Ni(OH)₂. Similarly, the reductive peak located at -790 mV is also characteristic of the reductive peak of nickel electrodes. Additionally, the absolute size of the electrode can be approximated using the data from the cyclic voltammogram. The absolute current values for the raw data are nearly identical to the absolute current values for the raw cyclic voltammogram data for Ni_{Black} electrodes indicating that the two types of depositions lead to similar size blacked nickel surfaces. Second, using the CO stripping area procedure discussed in Chapter 2, a real surface area of the electrode can be obtained. These real surface areas are identical to the usual surface areas calculated for Ni_{Black} electrodes using this method. All of these observations lead to the conclusion that, while platinum has unquestionably been deposited onto the electrode, it must certainly not be located on the surface, but rather present underneath the nickel deposit. Additionally, the presence of platinum in this form had no effect on the deposition potential, the size of the deposited electrode or the composition of the electrode surface.

4.3 Electrochemical Oxidation of 2-Propanol: In order to determine the activity, if any, of the co-deposited Ni+Pt electrodes towards the electrooxidation of 2-propanol, the same potentiodynamic and potentiostatic

experiments were carried out as before. Figure 4-6 shows the stabilized potentiodynamic response of the first co-deposited electrode towards the electrooxidation of 2-propanol in alkaline media. As with the cyclic voltammograms, all four conventionally co-deposited electrodes provided the same potentiodynamic response, so only the potentiodynamic response of the first co-deposited Ni+Pt electrode is shown.

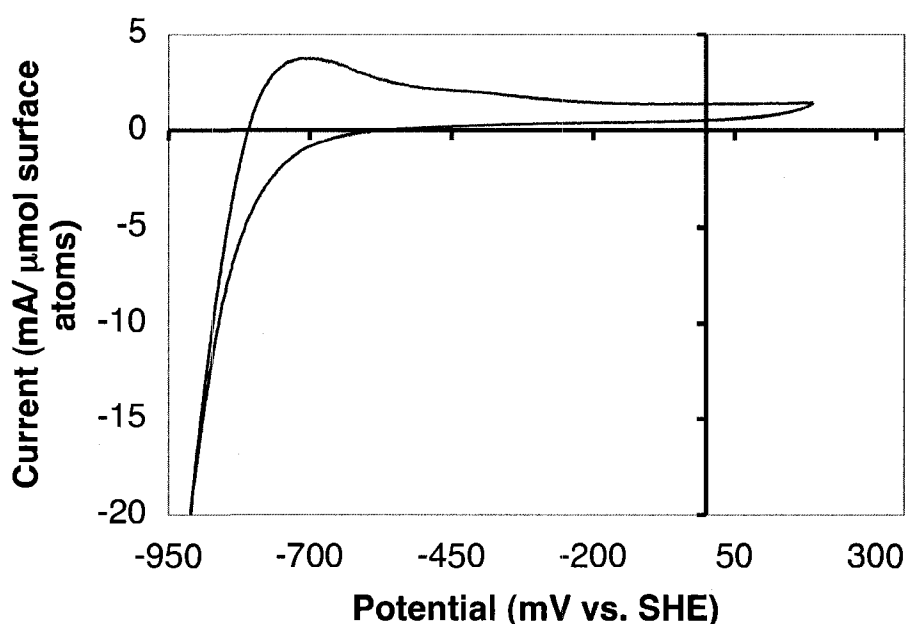


Figure 4-6: Potentiodynamic electrooxidation of 1 M 2-propanol in 0.5 M NaOH over a co-deposited Ni+Pt electrode.

The stabilized response is again characteristic of that of Ni_{Black} electrodes. At high potentials there is no increased current to indicate that 2-propanol is being consumed and at the lower potentials the response is typical of oxidizing nickel in alkaline electrolytes. As with Ni_{Black} electrodes, it can be

concluded that these co-deposited electrodes are not active towards the electrooxidation of 2-propanol.

Figure 4-7 shows the potentiostatic electrooxidation of 2-propanol over the co-deposited electrodes. Only the response of the first co-deposited Ni+Pt electrode is shown. The potentiostatic response was again identical to that of the Ni_{Black} electrodes.

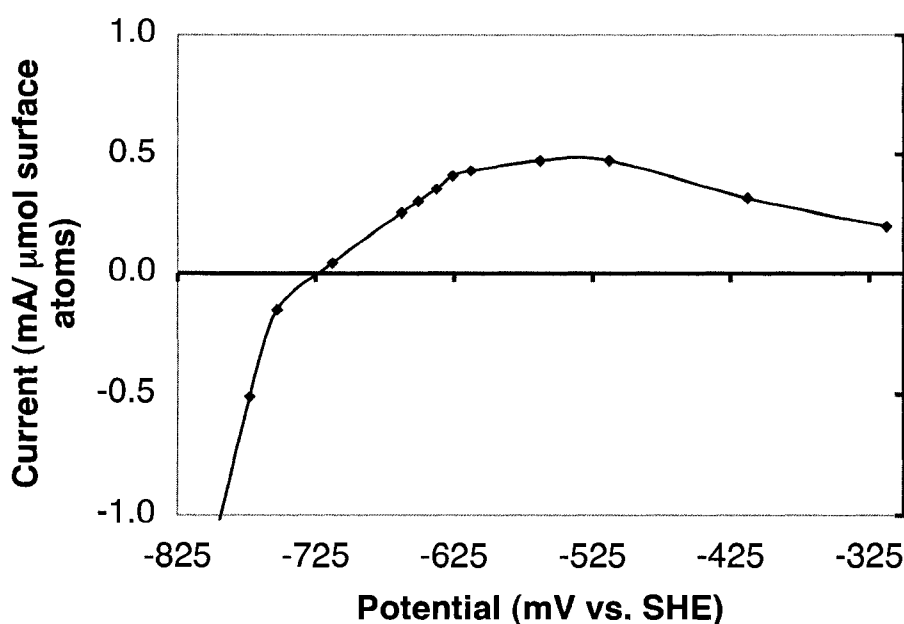


Figure 4-7: Potentiostatic electrooxidation of 1 M 2-propanol over a co-deposited electrode.

4.4 Conclusion: A conventional co-deposition method was used to prepare alternate Ni/Pt electrodes of approximately the same bulk composition as the original Ni/Pt electrodes. The deposition behaviors and voltammetric responses in the presence and absence of 2-propanol were, however, all

characteristic of the responses obtained using Ni_{Black} electrodes. The presence of platinum was confirmed during the deposition and on the electrode using ICP analysis and was present in concentrations greater than present with Ni/Pt electrodes. The co-deposited electrodes were inactive towards the electrooxidation of 2-propanol in alkaline media. We believe this to have occurred due to the relatively small amount of platinum being covered by nickel during the deposition process. As to why this behavior is not observed during the original deposition to form the original Ni/Pt electrodes is unclear.

Chapter 5: Future Work

Future work on this project will focus on three distinct areas: adaptation of this deposition procedure to make a compatible fuel cell electrode, more detailed characterization of the deposit, and further investigation into the mechanism of the deposition procedure.

Adaptation of the catalyst for fuel cell compatibility would primarily entail performing the deposition onto a support other than nickel gauze. This alternate support would be sized to fit the anode opening of the prototype fuel cell and be a material compatible with fuel cell operation. Carbon felt would be a good alternative support. The deposition procedure described in this thesis could easily be adapted for carbon felt support by simply changing the size of the deposition flask. Following this, the adapted Ni/Pt electrocatalyst could be mounted in an operational direct 2-propanol alkaline fuel cell where the cell performance and efficiency could be obtained.

Deposition onto a flat carbon felt surface, as opposed to a gauze, would make characterization of the deposit much easier. Detailed characterization is required to better understand the distribution of platinum on the surface of the electrode and the morphology of the deposit. SEM backscattering techniques would allow for the locations of platinum and nickel to be known in addition to revealing the nature of the surface. EDX analysis would also allow for better understanding of the elemental composition of the deposit.

Finally, it is important to better understand why the deposition occurs the way it does. Specifically, we wish to understand why the conventional co-deposition method does not produce an active platinum surface under the conditions explored in this thesis. Perhaps the use of platinum precursors with different ligand systems could produce deposits active towards the oxidation of 2-propanol. It would also be of interest to examine the role of the deposition solution in greater detail, specifically how the pH, applied deposition current, and deposition time affect the resulting Ni/Pt deposit.

Chapter 6: Experimental Procedures

General Procedures: Nitrogen (Praxair, prepurified), CO (Praxair, prepurified), NaOH (Alfa Aesar, 99.99%, semiconductor grade), H₂O₂ (EM Science, ACS Grade), H₂PtCl₆·6H₂O (Alfa Aesar, 99.9% metal basis), NiCl₂ (Aldrich), NH₄Cl (EMD Chemicals), platinum gauze (Alfa Aesar, 25 mm x 25 mm, 52 mesh woven from 0.1 mm diameter wire, 99.9% metal basis), platinum wire (Alfa Aesar, 25mm x 25 mm, 52 mesh woven from 0.1 mm diameter wire, 99.9% metal basis), nickel gauze (Alfa Aesar, 100 mesh woven from 0.1 mm diameter wire, 99.9% metal basis) and nickel wire (Alfa Aesar, 1 mm diameter wire, 99.9% metal basis) were used as received from supplier. The water was deionized, doubly distilled, and distilled again from alkaline KMnO₄ (Fisher Scientific) before use. 2-propanol (Fischer Scientific, suitable for electronic use) was freshly distilled. The calomel reference electrode was calibrated against a 1 M H₂SO₄ reference hydrogen electrode and a 0.5 M NaOH reference hydrogen electrode.

Electrochemical experiments were carried out on a Solartron model SI 1287 Potentiostat controlled with CorrWare version 2.3d software. Voltammetric readings were obtained using a RadioShack® 24-Range LCD Digital Multimeter with PC interface. Inductively Coupled Plasma (ICP) experiments

were performed on a Perkin Elmer Elan6000 quadrupole ICP-MS equipped with a Perkin Elmer AS-91 automated sampler.

Nickel Electrode Supports: 15 cm of 1 mm nickel wire was cut to length. Using pliers, one end was bent into a square with dimensions of approximately 1.5 cm x 1.5 cm. A square of nickel gauze, approximately 2 cm x 2 cm, was folded over the wire square. Both wire and gauze were pressed around the end of a pen to create a cylindrical shape that allowed the electrode to fit through the necks of round bottom flasks. The end of the nickel wire was flame sealed within a uranium glass shaft with a 3 mm diameter.

Blackened Platinum Gauze: A 15 cm length of 1 mm platinum wire was cut to length. Using pliers, one end was bent into a square of approximately 1.5 cm x 1.5 cm. A square of platinum gauze, approximately 2 cm x 2 cm, was folded over the wire square. Both wire and gauze were pressed around the end of a pen to create a cylindrical shape that allowed the electrode to fit through the necks of round bottom flasks. The end of the wire was flame sealed within a uranium glass shaft with a 3 mm diameter. The platinum electrode was cleaned in 1% H_2O_2 , followed by blackening in 2 wt.% $\text{H}_2\text{PtCl}_6 \cdot 6\text{H}_2\text{O}$ in 1 M HCl at 50 mV versus SHE with stirring for nine 20 minute installments totaling 3 hr. Between deposition installments, the platinum electrode was anodically polarized at -100 mV vs. SHE to clean the surface.

Cyclic Voltammograms: Under a N_2 atmosphere, a 100 ml, 3-neck round bottom flask was filled with 0.5 M NaOH and left to purge for at least 10 minutes prior to measurements. The reference electrode was a platinum-hydrogen electrode in the same alcohol-free electrolyte (RHE = -0.812 V vs. SHE) and the counter electrode was a blacked platinum gauze. The blacked platinum gauze was kept separate from the electrolyte by a 10 μm glass frit supported by a glass tube mounted through a punched rubber septum. The reference electrode was rinsed with triply distilled water and the working and the counter electrodes were cleaned in 2% H_2O_2 then rinsed with triply distilled water prior to measurements. The glass frit and counter electrode were submerged below the electrolyte level. The reference electrode and working electrode were then mounted through separate punched rubber septa and submerged below the degassed electrolyte. The working electrode was conditioned at -0.4 V vs. RHE for 5 minutes then cycled 3 times between -0.1 V and 0.425 V vs. RHE at a scan rate of 10 mV s^{-1} .

Galvanostatic Deposition of Pure Nickel Electrodes: The deposition apparatus consisted of two cylindrical glass containers joined at the bottom by a 10 μm glass frit. One chamber contained the basic nickel electrode and a saturated calomel electrode (SCE = 0.241 V vs. SHE). The second chamber contained a 2 cm x 2 cm carbon felt supported by a graphite holder, used as

the counter electrode to prevent platinum contamination. The reference electrode was rinsed with triply distilled water and the working and the counter electrodes were cleaned in 2% H_2O_2 then rinsed with triply distilled water prior to measurements. Both chambers were filled with a known volume of 0.2 M NiCl_2 / 2.0 M NH_4Cl . While stirring, a constant current of -0.1 A was applied to the working electrode for 1 hr. The potential of the counter electrode was recorded as a function of time using a multimeter.

Galvanostatic Deposition of Ni/Pt Electrodes: The deposition apparatus was a 9 cm tall glass cylinder with an inner diameter of 2.5 cm equipped with a stir bar. The counter electrode was a blacked platinum electrode and the reference electrode was a saturated calomel electrode. The reference electrode was rinsed with triply distilled water and the working and the counter electrodes were cleaned in 2% H_2O_2 then rinsed with triply distilled water prior to measurements. All three electrodes were submerged in a known volume of 0.2 M NiCl_2 / 2.0 M NH_4Cl and carefully positioned within the cylinder to prevent electrical contact. While stirring, a constant current of -0.1 A was applied to the working electrode for 1 hr. The potential of the counter electrode was recorded as a function of time using a multimeter.

Galvanostatic Deposition of Ni+Pt Electrodes: The deposition apparatus consisted of two cylindrical glass containers joined at the bottom by a 10 μm

glass frit. One chamber contained the basic nickel electrode and a saturated calomel electrode (SCE = 0.241 V vs. SHE). The second chamber contained a 2 cm x 2 cm carbon felt supported by a graphite holder, used as the counter electrode to prevent platinum contamination. The reference electrode was rinsed with triply distilled water and the working and the counter electrodes were cleaned in 2% H₂O₂ then rinsed with triply distilled water prior to measurements. Both chambers were filled with a known volume of 0.2 M NiCl₂ / 2.0 M NH₄Cl. To the chamber containing the working and reference electrode, a either 133 μL or 250 μL of 0.01438 M H₂PtCl₆ or 0.01520 M K[PtCl₃(C₂H₄)]•H₂O was added. While stirring, a constant current of -0.1 A was applied to the working electrode for 1 hr. The potential of the counter electrode was recorded as a function of time using a multimeter.

ICP Analysis of Deposition Aliquot Samples: During the depositions of the Ni, Ni/Pt, and Ni+Pt electrodes, 1 ml aliquot samples were taken from the deposition solution at 0,150, 300, 500, 700, 900, 1500, 2500, and 3600 seconds. These samples were diluted with 1 ml of 2% HNO₃ and submitted to the Radiogenic Isotope Facility for ICP analysis.

Potentiodynamic Electrooxidations of 1 M 2-Propanol in 0.5 M NaOH:

Under an atmosphere of N₂, a 100 ml, 3-neck round bottom flask, equipped with a dry ice/ acetone condenser, was filled with 90 ml of 0.5 M NaOH and

left to purge for at least 10 minutes prior to measurements. The reference electrode was a platinum-hydrogen electrode in the same alcohol-free electrolyte (RHE = -0.812 V vs. SHE) and the counter electrode was a blacked platinum gauze. The blacked platinum gauze was kept separate from the electrolyte by a 10 μm glass frit supported by a glass tube mounted in a punched rubber septum. The glass frit and counter electrode were submerged below the electrolyte level. The reference electrode was rinsed with triply distilled water and the working and the counter electrodes were cleaned in 2% H_2O_2 then rinsed with triply distilled water prior to measurements. The reference electrode and working electrodes were mounted through the same punched rubber septa and submerged below the degassed electrolyte. Once degassed, the electrolyte was heated to 60°C in a water bath atop a hot plate. At 60°C, 6.9 ml of freshly distilled 2-propanol was added to the electrolyte to make a 1 M 2-Propanol / 0.5 M NaOH solution. The solution was stirred vigorously for 30 seconds to ensure complete mixing. The working electrode was conditioned at -0.4 V vs. RHE for 5 minutes then cycled 3 times between -0.1 V and 1 V vs. RHE at a scan rate of 10 mV s^{-1} .

Potentiostatic Electrooxidations of 1 M 2-Propanol in 0.5 M NaOH: Under an atmosphere of N_2 , a 100 ml, 3-neck round bottom flask, equipped with a dry ice/ acetone condenser, was filled with 90 ml of 0.5 M NaOH and left to purge for at least 10 minutes prior to measurements. The reference electrode was a

platinum-hydrogen electrode in the same alcohol-free electrolyte (RHE = -0.812 V vs. SHE) and the counter electrode was a blacked platinum gauze. The blacked platinum gauze was kept separate from the electrolyte by a 10 μm glass frit supported by a glass tube mounted in a punched rubber septum. The glass frit and counter electrode were submerged below the electrolyte level. The reference electrode was rinsed with triply distilled water and the working and the counter electrodes were cleaned in 2% H_2O_2 then rinsed with triply distilled water prior to measurements. The reference electrode and working electrodes were mounted through the same punched rubber septa and submerged below the degassed electrolyte. Once degassed, the electrolyte was heated to 60°C in a water bath atop a hot plate. At 60°C 6.9 ml of freshly distilled 2-propanol was added to the electrolyte to make a 1 M 2-Propanol / 0.5 M NaOH solution, and stirred vigorously for 30 seconds to ensure complete mixing. The working electrode was conditioned at -0.4 V vs. RHE for 5 minutes and then held at a chosen potential for 15 minutes. The potentiostatic current after 15 minutes was calculated by averaging the current over the last 5 seconds of measurement.

CO Adsorption and Stripping: A new Ni/Pt electrode was prepared. Under an atmosphere of N_2 , a 100 ml, 3-neck round bottom flask was filled with 0.5 M NaOH and left to purge for 30 minutes prior to measurements. The reference electrode was a platinum-hydrogen electrode in the same alcohol-free

electrolyte (RHE = -0.812 V vs. SHE) and the counter electrode was a blacked platinum gauze. The blacked platinum gauze was kept separate from the electrolyte by a 10 μm glass frit supported by a glass tube mounted in a punched rubber septum. The glass frit and counter electrode were submerged below the electrolyte level. The reference electrode was rinsed with triply distilled water and the working and the counter electrodes were cleaned in 2% H_2O_2 then rinsed with triply distilled water prior to measurements. The reference electrode and working electrodes were then mounted in the same punched rubber septa and submerged below the degassed electrolyte. While bubbling $\text{N}_{2(\text{g})}$ through the electrolyte, the working electrode was conditioned at -0.4 V vs. RHE for 30 minutes with stirring. After 30 minutes, the nitrogen stream was pulled out of the electrolyte and blown over the surface while the working electrode was cycled 3 times between -0.1 V and 1.1 V (vs. RHE) at a scan rate of 10 mV s^{-1} to obtain a hydrogen baseline cyclic voltammogram.

CO adsorption and stripping were done by bubbling $\text{CO}_{(\text{g})}$ through the electrolyte while conditioning the working electrode at -0.4 V (vs. RHE) for 30 minutes with stirring. After 30 minutes, without degassing, the CO stream was pulled out of the electrolyte and blown over the surface while the working electrode was cycled 3 times between -0.1 V and 1.1 V (vs. RHE) at a scan rate of 10 mV s^{-1} .

ICP Analysis of the Deposit: The electrode was placed in a ceramic evaporating dish on a hot plate in a well-ventilated fume hood. To the dish, 30 ml of aqua regia (1:3, HNO₃:HCl) was added and the hot plate was heated to 100°C while the electrode was left to dissolve for 1 hr. After 1 hr, the wire mesh and a small amount of the nickel wire support had dissolved. The remaining wire support was removed from the acid bath. The wire was rinsed with triply distilled water and the waste was allowed to drip back into the evaporating dish. The dissolved metals remained on the hot plate at 100°C until the liquid had completely evaporated. The hot plate was turned off and the deposit was left to cool. The dried salts were dissolved in a small volume of triply distilled water, quantitatively transferred to a 50 ml volumetric flask, diluted to volume in 2% HNO₃, and submitted to the Radiogenic Isotope Facility for ICP analysis.

Chapter 7: References

- ¹ www.tatanano.com
- ² P. Aldhous, *Nature*, 435 (2005) 1152-1154.
- ³ http://nobelprize.org/nobel_prizes/peace/laureates/2007/index.html
- ⁴ IPCC, 2007: Summary for Policymakers. In: *Climate Change 2007: The Physical Science Basis. Contribution of Working Group I to the Fourth Assessment Report of the Intergovernmental Panel on Climate Change* [S. Solomon, D. Qin, M. Manning, Z. Chen, M. Marquis, K.B. Avery, M. Tignor and H.L. Miller (eds.)] Cambridge University Press, Cambridge, United Kingdom and New York, NY, USA.
- ⁵ A.J. Appleby, F.R. Foulkes, *Fuel Cell Handbook*, Van Nostrand Reinhold, New York, 1989.
- ⁶ M.L. Perry, T.F. Fuller, *J. Electrochem. Soc.*, 149 (2002) S59-S67.
- ⁷ T.S. Zhao, K.D. Kreuer, T. van Nguyen, *Advances in Fuel Cells*, Elsevier, Oxford, 2007.
- ⁸ F. Barbir, *PEM Fuel Cells: Theory and Practice*, Elsevier Academic Press, San Diego, 2005.
- ⁹ S. Dunn, *Int. J. Hydrogen Energ.*, 27 (2002) 235-264.
- ¹⁰ C. Song, *Catal. Today*, 77 (2002) 17-49.
- ¹¹ E. Chen, in: *Fuel Cell Technology Handbook*, Ed. Hoogers, G. CRC Press, Boca Raton, Fla., 2003.
- ¹² J.O. Bockris, S. Srinivasan, *Fuel Cells: Their Electrochemistry*, McGraw-Hill Book Company, New York, 1969.
- ¹³ W.R. Grove, *Philos. Mag.* 127 (1839).
- ¹⁴ W. Ostwald, *Z. Elektrochem.*, 1, 122 (1894).
- ¹⁵ F.T. Bacon, *J. Electrochem. Soc.* 126 (1979) 7C-17C.
- ¹⁶ B. Viswanathan, M. Aulice Scibioh, *Fuel Cells: Principles and Applications*, CRC Press, Boca Raton, 2007.
- ¹⁷ G. Crawley, "Alkaline Fuel Cells (AFC)" *Fuel Cell Today* (March 2006) www.fuelcelltoday.com
- ¹⁸ K. Rajashekara, *IEEE Trans. Ind. Appl.*, 30 (1994) 897-904.
- ¹⁹ F. Barbir, S. Yazici, *Int. J. Energy Res.*, 32 (2008) 369-378.
- ²⁰ G. Hoogers, in: G. Hoogers (Ed.), *Fuel Cell Technology Handbook*. CRC Press, Boca Raton, Fla. 2003
- ²¹ J. Larminie, A. Dicks, *Fuel Cell Systems Explained*, Wiley, New York, 2000.
- ²² R.K. Shah, in: S. Basu (Ed.), *Recent Trends in Fuel Cell Science and Technology*, Springer, New York, 2007.
- ²³ G. Cawley, "Proton Exchange Membrane (PEM) Fuel Cells" *Fuel Cell Today* (March 2006) www.fuelcelltoday.com
- ²⁴ S. Litster, G. McLean, *J. Power Source* 130 (2004) 61-76.
- ²⁵ A.L. Dicks, *J. Power Source* 61 (1996) 113-124.

-
- ²⁶ L. Barelli, G. Bidini, F. Gallorini, S. Servili, *Energy* 33 (2008) 554-570.
- ²⁷ J-H. Wee, K-Y. Lee, *J. Power Source* 157 (2006) 128-135.
- ²⁸ G.F. McLean, T. Niet, S. Prince-Richard, N. Djilali, *Int. J. Hydrogen Energ.* 27 (2002) 507-526.
- ²⁹ S.R. Choudhury, in: S. Basu (Ed.), *Recent Trends in Fuel Cell Science and Technology*, Springer, New York, 2007.
- ³⁰ N. Sammes, R. Bove, K. Stahl, *Curr. Opin. Solid State Mater. Sci.*, 8 (2004) 372-378.
- ³¹ http://www.wd.gc.ca/77_4600_ENG_ASP.asp
- ³² G. Cawley, "Molton Carbonate Fuel Cells" *Fuel Cell Today* (March 2007) www.fuelcelltoday.com
- ³³ H. Ghezal-Ayagh, M. Farooque, H.C. Maru, in: S. Basu (Ed.), *Recent Trends in Fuel Cell Science and Technology*, Springer, New York, 2007.
- ³⁴ G. Cawley, "Solid Oxide Fuel Cells (SOFC)" *Fuel Cell Today* (January 2007) www.fuelcelltoday.com
- ³⁵ S.M. Haile, *Acta. Mater.* 51 (2003) 5981-6000.
- ³⁶ S. Wasmus, A. Kuver, *J. Electroanal. Chem.*, 461 (1999) 14-31.
- ³⁷ G. Cawley, "Direct Methanol Fuel Cell (DMFC)" *Fuel Cell Today* (August 2007) www.fuelcelltoday.com
- ³⁸ X. Ren, P. Zelenay, S. Thomas, J. Davey, S. Gottesfeld, *J. Power Source*, 86 (2000) 111-116.
- ³⁹ <http://www.mtimicrofuelcells.com/technology/breakthrough.asp>
- ⁴⁰ A. Heinzl, V.M. Barrgan, *J. Power Source*, 84 (1999) 70-74.
- ⁴¹ V. Neburchilov, J. Martin, H. Wang, J. Zhang, *J. Power Source*, 169 (2007) 221-238.
- ⁴² J.R. Varcoe, R.C.T. Slade, *Fuel Cells*, 5 (2005) 187-200.
- ⁴³ J.S. Spendelow, A. Wieckowski, *Phys. Chem. Chem. Phys.*, 9 (2007) 2654-3675.
- ⁴⁴ K. Scott, E. Yu, G. Vlachogiannopolos, M. Shivare, N. Duteanu, *J. Power Source* 175 (2008) 452-457.
- ⁴⁵ D. Cao, S.H. Bergens, *J. Power Source*, 124 (2003) 12-17.
- ⁴⁶ M.E.P. Markiewicz, D.M. Hebert, S.H. Bergens, *J. Power Source*, 161 (2006) 761-767.
- ⁴⁷ C.K. Ralph, S.H. Bergens, *Organometallics*, 26 (2007) 1571-1574.
- ⁴⁸ Calculated from values obtained from D.R. Lide, *CRC Handbook of Chemistry and Physics* 86th ed., CRC Press, Boca Raton, Fla., 2005
- ⁴⁹ H. Lui, C. Song, L. Zhang, J. Zhang, H. Wang, D.P. Wilkinson, *J. Power Source*, 155 (2006) 95-110.
- ⁵⁰ T. Frelink, W. Visscher, J.A.R. van Veen, *Surf. Sci.*, 335 (1995) 353-360.
- ⁵¹ E. Antolini, J.R.C. Salgado, E.R. Gonzalez, *J. Electroanal. Chem.*, 580 (2005) 145-154.
- ⁵² E. Antolini, *Electrochem. Solid State Lett.*, 8 (2005) A226-A230.

-
- ⁵³ J. Mathiyarasu, A.M. Remona, A. Mani, K.L.N. Phani, V. Yegnaraman, J. Solid State Electrochem., 8 (2004) 968-975.
- ⁵⁴ J.F. Drillet, A. Ee, J. Friedemann, R. Kotz, B. Schnyder, V.M. Schmidt, Electrochim. Acta., 47. (2003) 1983-1988.
- ⁵⁵ H. Yang, C. Coutanceau, J.M. Leger, N. Alonso-Vante, C. Lamy, J. Electroanal. Chem. 576 (2005) 305-313.
- ⁵⁶ H.R. Colón-Mercado, H. Kim, B.N. Popov, Electrochem. Comm., 6 (2004) 795-799.
- ⁵⁷ V. Stamenkovic, T.J. Schmidt, P.N. Ross, N.M. Markovic, J. Electroanal. Chem., 554-555 (2003) 191-199.
- ⁵⁸ M.A.A. Rahim, H.B. Hassan, R.M. Abdel Hameed, Fuel Cell, 4 (2007) 298-305.
- ⁵⁹ N. Martz, C. Roth, H. Fueb, J. Appl. Electrochem., 35 (2005) 85-90.
- ⁶⁰ M. Goetz, H. Wendt, J. Appl. Electrochem., 31 (2001) 811-817.
- ⁶¹ K.W. Park, J.H. Choi, S.A. Lee, C. Pak, H. Chang, Y.E. Sung, J. Catal., 224 (2004) 236-242.
- ⁶² J.H. Choi, K.W. Park, B.K. Kwon, Y.E. Sung, J. Electrochem. Soc., 150 (2003) A973-A978.
- ⁶³ K.W. Park, J.H. Choi, B.K. Kwon, S.A. Lee, Y.E. Sung, J. Phys. Chem. B, 106 (2002) 1869-1877.
- ⁶⁴ T. Toda, H. Igarashi, H. Uchida, M. Watanabe, J. Electrochem. Soc., 146 (1999) 3750-3756.
- ⁶⁵ K.W. Park, J. H. Choi, Y.E. Sung, J. Phys. Chem. B, 107 (2003) 5851-5856.
- ⁶⁶ Y. Liang, H. Zhang, Z. Tian, X. Zhu, X. Wang, B. Yi, J. Phys Chem. B, 110 (2006) 7828-7834.
- ⁶⁷ S. Mukerjee, S. Srinivasan, J. Electroanal. Chem., 357 (1993) 201-224.
- ⁶⁸ R. Woods, Electroanal. Chem. Interfacial Electrochem., 49 (1974) 217-226.
- ⁶⁹ M.M. Jaksic, B. Johansen, R. Tunold, Int. J. Hydrogen Energ., 18 (1993) 817-837.
- ⁷⁰ C.A. Marozzi, A.C. Chialvo, Electrochim. Acta., 45 (2000) 2111-2120.
- ⁷¹ B. Rosenberg, L. Van Camp, T. Krigas, Nature, 205 (1965) 698-699.
- ⁷² I.M. Kolthoff, E.B. Sandell, Textbook of Quantitative Inorganic Analysis, third ed., 406 (Macmillan Co.; New York, 1952)
- ⁷³ A.P. Yadev, A. Nishikata, T. Tsuru, Electrochim. Acta., 52 (2007) 7444-7452
- ⁷⁴ K. Matsuoka, S. Sakamoto, K. Nakato, A. Hamada, Y. Itoh, J. Power Source, 179 (2008) 560-565.
- ⁷⁵ E. Guilminot, A. Corcella, F. Charlot, F. Maillard, M. Chatenet, J. Electrochem. Soc., 154 (2007) B96-B105.
- ⁷⁶ D.C. Johnson, D.T. Napp, S. Bruckenstein, Electrochim. Acta., 15 (1970) 1493-1509.
- ⁷⁷ J.S. Spendelow, A. Wieckowski, Phys. Chem. Chem. Phys., 9 (2007) 2654-2675.

-
- ⁷⁸ F. Hahn, B. Beden, M.J. Croissant, C. Lamy, *Electrochim. Acta.*, 31 (1986) 335-342.
- ⁷⁹ F. Hahn, D. Floner, B. Beden, C. Lamy, *Electrochim. Acta.*, 32 (1987) 1631-1636.
- ⁸⁰ S.A.S. Machado, L.A. Avaca, *Electrochim. Acta.*, 39 (1994) 1385-1391.
- ⁸¹ D. Cao, Nanoparticle Pt-Ru adatom catalysts for direct methanol fuel cells; The study of a direct 2-propanol polymer electrolyte fuel cell, PhD Thesis, University of Alberta, 2004.
- ⁸² R.K. Shervedani, A. Lasia, *J. Appl. Electrochem.*, 29 (1999) 979-986.
- ⁸³ J.S. Spendelow, G.Q. Lu, P.J.A. Kenis, A. Wieckowski, *J. Electroanal. Chem.*, 568 (2004) 215-224.
- ⁸⁴ C.H. Chang, T.C. Wen, *Mater. Chem Phys.*, 47 (1997) 203-210.
- ⁸⁵ M. Grden, K. Klimek, *J. Electroanal. Chem.*, 581 (2005) 122-131.
- ⁸⁶ M. Grden, K. Klimek, A. Czerwinski, *J. Solid State Electrochem.* 8 (2004) 390-397.
- ⁸⁷ A. Seghioer, J. Chevalet, A. Barhoun, F. Lantelme, *J. Electroanal. Chem.* 442 (1998) 113-123.
- ⁸⁸ A. Seyeux, V. Maurice, L.H. Klein, P. Parcus, *J. Solid State Electrochem.* 9 (2005) 337-346.
- ⁸⁹ C.V. D'Alkaine, M.A. Santanna, *J. Electroanal. Chem.* 457 (1998) 5-12.
- ⁹⁰ Z.I. Kudryavtseva, L.A. Burkal'tseva, A.G. Pshenichnikov, *Russ. J. Electrochem.* 40 (2004) 1208-1213.